UNIVERSITY OF SOUTHAMPTON

Foil Performance of a Flapping Foil Wave Propelled Vessel

Andrea Chipolina

Thesis Supervisor: Nicholas Townsend

Second Marker: Jon Downes

Submitted to the Faculty of Engineering and Physical Sciences in partial fulfilment of the requirements for the degree of:

MSc Maritime Engineering Science / Computational Fluid Dynamics

at the

University of Southampton

September 2020

'This thesis was submitted for examination in September 2020. It does not necessarily represent the final form of the thesis as deposited in the university after examination.'

I, Andrea Chipolina declare that this thesis and the work presented in it are my own and has been generated by me as the result of my own original research.

I confirm that:

1. This work was done wholly or mainly while in candidature for a degree at this University;

2. Where any part of this thesis has previously been submitted for any other qualification at this University or any other institution, this has been clearly stated;

3. Where I have consulted the published work of others, this is always clearly attributed;

4. Where I have quoted from the work of others, the source is always given. With the exception of such quotations, this thesis is entirely my own work;

5. I have acknowledged all main sources of help;

6. Where the thesis is based on work done by myself jointly with others, I have made clear exactly what was done by others and what I have contributed myself;

7. None of this work has been published before submission.

Foil Performance of a Flapping Foil Wave Propelled Vessel

MSc Project

Andrea Chipolina
MSc Maritime Engineering; Fluid Dynamics
University of Southampton

ABSTRACT This study provides insight on the improvement of propulsion efficiency of a wave propelled autonomous vehicle. The aim of this project is to investigate the influence of wave orbital motion and foil interaction on aft foil performance, of pitch driven wave propelled flapping foils. The evaluation is carried out for two 2D NACA0012 foils in tandem configuration, at varying interfoil spacing. An initial simplified numerical method has been developed with the use of potential flow theory. Resulting in the definition of a combined incoming flow including wave orbital velocity and vessel forward speed. Results obtained show the evaluation of wake development and a minimum interfoil spacing of 100% $_{(1/2LWL\ from\ LCG)}$ for foil interaction to be considered negligible. The study is then continued with the completion of a transient 2D RANS computational simulation with the use of Ansys Fluent (CFD). Showing a visual representation of the flow as the foils pitch and heave. Furthermore, results obtained show considerable improvement in aft foil performance for a small increase in pitch motion.

Keywords: hydrofoil theory; marine propulsion; wake; orbital motion; foil performance

TABLE OF CONTENTS

LIST OF TABLES

LIST OF GRAPHS

LIST OF FIGURES

ABBREVIATIONS

2D	Two dimensional
3D	Three dimensional
An	Analytical
AP	Aft perpendicular
ASV	Autonomous surface vehicle
CFD	Computational fluid dynamics
Deg	Degrees
Dir	Direction
Exp	Experimental
FP	Forward perpendicular
Fwd	Forward
ITTC	International Towing Tank Committee
LCG	Longitudinal centre of gravity
Num	Numerical
RANS	Reynolds-Averaged Navier-Stokes
RNG	Re-Normalisation Group
Sim	Simulation

NOMENCLATURE

a	Wave amplitude	m
A	Foil pivot point	-
c	Foil chord	m
C_D	Foil drag coeffcient	-
c_f	Turbulent friction coefficient	-
C_F	Total friction coefficient	-
C_L	Foil lift coefficient	-
$C_{L\alpha}$	Lift coefficient slope	-
C_T	Thrust coeffcient	-
d	Body diameter	m
D	Drag	N
Fr	Froude number	-
Fx	Force in the x-direction acting on the foil	N
Fy	Force in the y-direction acting on the foil	N
g	Gravitational acceleration	Nms^{-2}
h_i	Foil heave	m
H_i	Foil depth	m
i	Foil number	-
j	Panel number	-
k	Wave number	-
L	Lift	N
L_{WL}	Vessel waterline length	m
N	Total number of panels	-
Q	Torque	N.m
Re	Reynolds number	-
s	Interfoil spacing	m
S	Panel surface	m^2
T	Thrust	N
t	Time	s
	Foil thickness	m
T_f	Flapping period of foil	s
T_w	Wave period	s
$\overline{T}$	Average thrust	N
Tx	Total resultant foil force in x-direction	N

U	Freestream velocity	m/s
u^*	Friction velocity	m/s
u_0	Amplitude of the wave-induced fluid particle velocity	-
$U1$	Wake velocity defect	m/s
U_{aft}	Flow velocity encountered by aft foil	m/s
U_{com}	Combined incoming flow	m/s
U_{sep}	Flow velocity at separation	m/s
U_{vess}	Mean vessel forward speed	m/s
u_w	Horizontal components of fluid velocities	m/s
U_{wake}	Flow velocity at foil wake	m/s
u_x	Wavy flow inlet velocity x-component	m/s
u_y	Wavy flow inlet velocity y-component	m/s
$\overline{Vel}_{inlet}$	Average velocity inlet	m/s
V_i	Inflow velocity	m/s
v_w	Vertical components of fluid velocities	m/s
W	Wake width	m
x	Global x axis coordinate	-
y	Global y axis coordinate	-
Y_1	Distance of the first cell centre to the wall	m
Y_+	Wall Y-plus- wall-normal distance of the centre of the first grid	-
α_i	Foil angle of attack	deg.
ε	downwash angle	deg.
θ_i	Foil pitch angle	deg.
λ	Wavelength	m
μ	Fluid dynamic viscocity	Pa.s
ν	Fluid kinematic viscocity	m^2/s
ρ	Fluid density	kgm^{-3}
σ	Boundary layer thickness	m
τ_w	Wall shear stress	Pa
Υ	Panel vortex strength	m/s
ψ	Wave-phasing parameter	rad
ω	Wave frequency	rad

1. INTRODUCTION

The evolution of marine propulsion systems shows a clear shift from the use of renewable resources to the use of fossil fuels, as the marine steam engine was introduced in the early 19th Century. The use of mechanical systems brought attention to the design of efficient propulsion types; from the paddle wheel, to the screw propeller and the water jet. The optimization of propulsion systems remains a popular topic area of investigation, with the intention to reduce operational costs, duration of voyages and environmental impact.

The current urgency to reduce environmental impact has triggered an interest in the use of renewable energy in the marine industry. Recent examples are the latest merchant ships, with the incorporation of kites, offering the possibility to reduce fuel consumption by 20%. Furthermore, companies such as Wavefoil propose the inclusion of retractable bow foils that could save 5-15% of fuel. Moreover, Autonaut produces autonomous vehicles propelled by pitch induced flapping foils in tandem. Causing zero emissions and requiring minimal assistance.

The main topic area of this study is on the use of wave energy as a method of propulsion for autonomous vehicles. Focusing on the hydrodynamic aspects of flapping foils in tandem. An extensive literature review was undertaken, providing insight on further work required on the subject matter. Foils in tandem improve vessel stability and solve the issue of inconsistent thrust faced by a single foil. However, the aft foil is operating in forward foil wake, causing a reduction in efficiency. Various investigations provide insight in the optimization of thrust with respect to; wake, vessel pitching motion, wave orbital motion or foil geometry.

However, the use of pitch driven flapping foils in tandem on marine vehicles involves all factors. Interfoil spacing is a variable in common, in existing publications, that can drastically affect vessel motion and propulsion efficiency. Thus, it is believed that there is a need to investigate a combination of these factors, providing insight on the hydrodynamics involved in the use of tandem flapping foils and the effect of interfoil spacing on aft foil performance.

The first stage of the analysis involves the completion of a 2D simplified numerical simulation based on potential flow theory. Providing wake development, lift and drag coefficients of both foils. Trends are obtained for a range of wave frequencies and interfoil spacings. Results show particular interest in foil performance at a wave frequency of 4 radians. Suggesting the possibility to achieve a foil configuration that satisfies all flow components.

The second stage of the analysis includes a continuation of the study in more detail with the use of computational fluid dynamics (Ansys Fluent). A 2D RANS transient simulation was completed, with an incoming wave of 4 radians. Two sets of results were

obtained including prescribed foil flapping motion based on experimental data and an equal pitch motion of +/- 14 deg. The data obtained show average thrust generation of each foil along with visual representations of the flow.

The article continues with a brief description on the literature review, followed by the dynamics of the problem and the analysis undertaken.

2. LITERATURE REVIEW

The possibility of thrust generation with the use of flapping foils has been considered for over a century. Early investigations include the study of harmonically heaving foils by Knoller and Betz (Jones, K. D. 1998). Where the identification of lift generated by a foil in uniform flow, at an angle of attack is presented. These findings, so called the Knoller-Betz effect, were further exploited by Katzmayr (1922). who showed that an oscillating foil in uniform flow also produces thrust.

Similar topic areas such as; the 'The General Theory of Aerodynamic Instability and the Mechanism of Flutter' by Theodorsen, T. (1949) resulted in a major contribution for this on-going investigation, where a solution involving potential flow and the adoption of the Kutta condition, is presented. The mathematical theory developed by Theodorsen, T. (1949) was then enhanced by I.E.Garrick. (1936) with the publication of 'Propulsion of a Flapping and Oscillating Airfoil'. These advances in research, amongst others, have allowed for the study of a possible evolution in marine propulsion mechanisms.

Moreover, it must be noted that all systems intended to propel through a fluid, have been very much influenced by nature. Aquatic locomotion being a major influence in marine propulsion. Lighthill, J. (1975) addresses the biofluiddynamic behavior of several aquatic animals. These findings have been referred to in the design of numerous propulsion devices. Alternatively, these studies have allowed for the design of devices to reduce vessel motion and improve seakeeping, such as stern foils acting as dampers.

These concepts were considered further by Yamaguchi, H., & Bose, N. (1994). Where both rigid and partly flexible oscillating stern foils were examined, proposing linear and non-linear theories. Results showed a 5% increase in propulsive efficiency in comparison to the screw propeller. Meanwhile, Bøckmann, E. (2016) showed that it is possible to achieve 5-15% fuel savings by installing actively pitch controlled foils on ships.

Due to its similarity in purpose, most existing publications on oscillating foil hydrodynamics refer to the use of foils in turbines for energy harvesting. A clear example is the study of 'Optimal Tandem Configuration for Oscillating Foils Hydrokinetic Turbine' by Dumas, G. (2012) A computational fluid dynamics simulation was carried out, exploring the effect of foil spacing. Results

Publication	Factors considered	Method
Yamaguchi, H. (2012)	x	CFD
Epps, B. P. (2017)	▪	CFD & Experimental
Hugli, W. C. (1954)	x ▪	Theory & Experimental
Bowker, J. A. (2018).	x ∫	Numerical & Experimental

Wave orbital motion x
Forward foil wake ▪
Vessel coupled dynamics ∫

Table 1: Primary publications

showed that *"favorable interactions between the downstream foil and the wake vortices may lead to unexpectedly high power-extraction efficiencies (up to 64%), while unfavorable interactions may cause the downstream foil to contribute negatively to the total power extracted."* [1]

Epps, B. P. (2017) further highlighted the effects of foil interaction of oscillating foils in tandem, and the effects of phase lag and interfoil spacing on propulsion efficiency. A new non-dimensional parameter was proposed that relates foil spacing with aft foil performance. Furthermore, the wake produced by the forward foil will depend not only on the conditions the system operates at, but also forward foil geometry. Investigations such as; Xie, Y. (2019) show the need for a leading edge vortex to obtain lift and the influence of varying foil thickness in the use of oscillating foils in tandem for energy harvesting.

The above-mentioned investigations consider a flow field composed of incoming uniform flow and the resultant forward foil wake. However, when considering the use of wave augmented flapping foils, the wave orbital motion must be taken into consideration. Paul Kaplan was among the first scientists to propose a theoretical analysis on 'Two-Dimensional Wake and Downwash of a Hydrofoil in Waves.' Hugli, W. C. (1954). The theoretical analysis proposed resulted in the conclusion that *"the resultant downwash angle and its rate of change, are the sum of the contribution found for the case of motion under an undisturbed free surface and a sinusoidal time-dependent component due to the sea wave influence."* [2]

A more recent investigation, by Yamaguchi, H. (2012) investigated the extraction of energy from gravity waves by completing a numerical simulation of a 2D oscillating hydrofoil with the use of Fluent. The discussion presented highlights the effect of phase difference between wave and foil motion and its influence in thrust generation. Showing that a wave phase difference of +/- 90 deg. is desired to achieve maximum thrust and propulsion efficiency.

Two final references for this project are recent publications; Gauthier, M (2018) and Bowker, J. A. (2018). The first study presents a theoretical, numerical and experimental

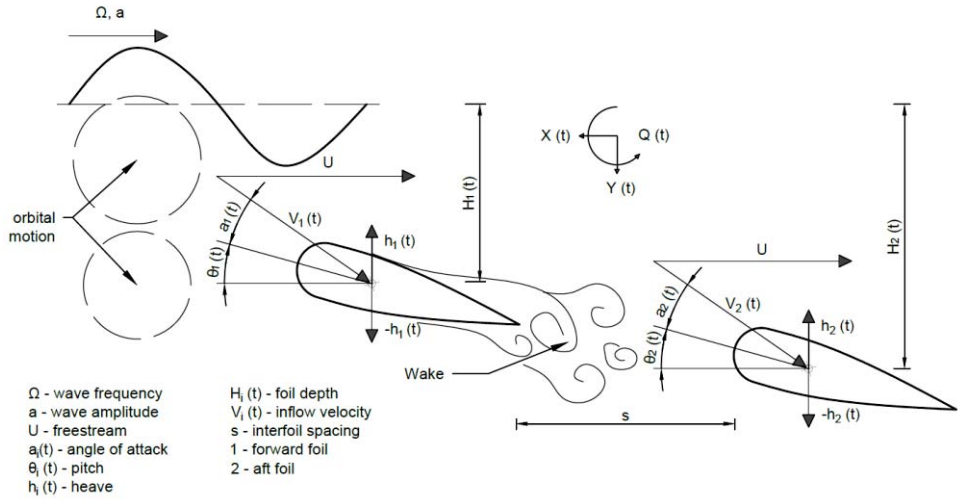

Fig. 1: Diagrammatic representation of two foils in tandem

approach towards the analysis of motion and hydrodynamics of an ASV. Interesting visualizations of the forward foil wake, carried out with the use of CFD software packages, show that *"the wake pattern appears similar to a classic von Kármán street"*. [3]

The data presented, especially those obtained theoretically and numerically, are of use. However, the experimental platform is simplified to a foil supported by a rig, which is then placed onto a towing tank carriage. In order to obtain results closely related to the motions encountered by an ASV, the foils must be installed onto a model to allow for free running experiments.

This problem is resolved by Bowker, J. A. (2018), where experimental testing of a wave powered ASV is carried out. A numerical and experimental approach was followed, to predict free running forward speed of pitch-driven wave propelled vessels. Throughout testing, observations are made varying; wave frequency, wave amplitude and foil spacing. The results obtained show the evaluation of; free running wave propulsion response, the effect of foil location on the coupled dynamics and flapping response of both foils.

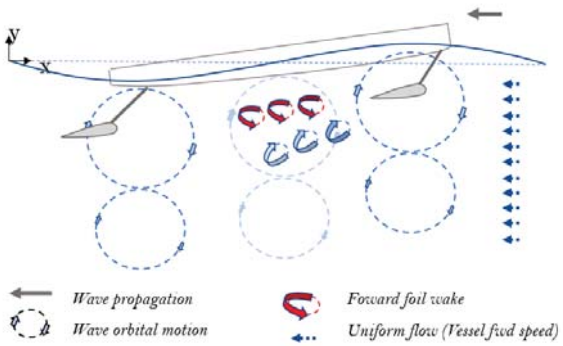

Fig. 2: Hydrodynamic components

To conclude the literature review, the extensive list of publications considered has been reduced to the main papers that will be directly referred to throughout the completion of calculations, experimental testing and the evaluation of results. An important area investigated in each study has been identified, along with factors not considered that are required for the completion of this project. *Table 1* shows how each publication is relevant to the definition of this project. Further detail on

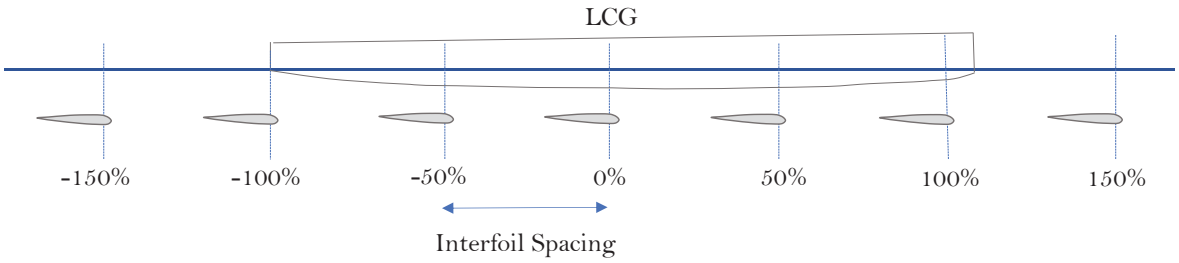

Fig. 3: Range of interfoil spacing

important parameters evaluated in each publication are shown in *Table 7*$_{(Appendix A)}$. *Fig. 2* shows the main components considered in the analysis.

3. DYNAMICS

Fig 1. illustrates the foil configuration and a kinematic representation of the analysis. The main variable being interfoil spacing 's'. Heave and pitch motions have been defined as sine functions, simulating motions obtained during experimental testing with the use of an ASV, at the specified wave frequency.

The motion of the foils result in x-dir. and y-dir. forces ($X_{(t)}$,$Y_{(t)}$) along with a torque acting at the foil pivot point ($Q_{(t)}$). All components are time-varying and a function of incoming wave frequency. Interfoil spacing ranges from 50%-150% $_{(1/2LWL\ from\ LCG)}$, as shown in *Fig. 3*.

4. AIM AND OBJECTIVES

The completion of extensive research has allowed for the identification of three components that must be considered in the analysis of the specified propulsion system. These include the following, previously investigated by above mentioned publications;

- Forward foil wake
- Wave orbital motion
- Vessel pitch motion

Each publication proposes insight on the optimal interfoil spacing with respect to the component analysed. The project proposed, involves understanding the combination of all three components. Thus, requiring the investigation of a possible optimal spacing value or range that will satisfy all components. An optimal spacing considering wave orbital motion and vessel pitch motion was investigated by Bowker, J. A. (2018). However, due to the choice of a considerably large interfoil spacing, foil interaction was considered negligible.

As stated in Epps, B. P. (2017), it is possible to achieve a favourable foil interaction that will cause higher aft foil efficiency whilst operating in forward foil wake, in uniform flow. The purpose of this investigation is to evaluate whether this is still possible when considering vessel forward motion and wave orbital motion. Thus, the aim of this project is to investigate the influence of wave orbital motion and foil interaction on aft foil

performance, of pitch driven wave propelled flapping foils. This will allow for the consideration of foil interaction and wave orbital motion in the design and identification of an optimal setup of flapping foils in tandem. *Fig. 1* showing a diagrammatic representation of the problem to be solved. *Fig. 2* shows the basic mechanisms for pitch-induced wave propulsion.

Two methods have been identified for the completion of this study. The first being a simplified numerical simulation based on potential flow theory. With the objective to obtain expected trends for a range of wave frequency and interfoil spacing. The analysis is continued with the use of computational fluid dynamics (Ansys Fluent). Where a specific scenario is evaluated further. *Table 2,* shows the particulars required.

Particulars	
Vessel waterline length, L_{WL}	*2.27 m*
Vessel longitudinal centre of gravity, L_{CG}	*-0.156 m (from amidships)*
Interfoil spacing range, s%	*50%, 80%, 110% & 140%*
Foil type	*NACA0012*
Foil chord, c	*0.23 m*
Pivot point,A	*Leading edge*
Fluid type	*Seawater*
Fluid temperature, T	*15˚C*
Fluid density, ρ	*1026.021 kg/m3*
Fluid dynamic viscocity, μ	*0.00122 Pa.s*

Table 2: Particulars

5. SIMPLIFIED NUMERICAL SIMULATION

5.1 Method

The simplified numerical analysis has been carried out as a Python Jupyter Notebook. The foil type analysed is a 2D NACA0012 foil, for which foil chord is the main input parameter. The code has been set as a tool allowing for the analysis of any symmetric NACA foil in wavy flow. However, theorems used involve certain assumptions and limitations described below:

Assumptions:

- Deep water
- Small amplitude waves
- 2D Geometry
- Hull interaction negligible

Limitations:

- Head waves
- Max foil pitch angle; +/- 14 deg.
- Doppler effect excluded

Restricting pitch angles to a maximum of 14 deg. is a key limitation of this method. High angles of attack can cause highly turbulent flow resulting in inappropriate use of 2D potential flow theory. Furthermore, the use of XFOIL MIT. (2019) was required to provide drag coefficient values. At angles greater than 14 deg. the solution would not reach convergence.

Linear wave theory was implemented with the use of *Eqn.1 to 3,* described in *Fig.4.* Where values required include wave number and frequency ‘k’,’ω’. Foil height ‘h’ dependent on heave motion. Horizontal and vertical velocity components are also a function of distance travelled in the x-dir. ‘x’. Thus, the velocity encountered by the forward foil varies in the x and y direction. Allowing for the calculation of the amplitude of the wave-induced fluid particle velocity

'u_0' and the horizontal and vertical components of such, 'u_w' and 'v_w'

$$u_o = \frac{gka}{\omega}.exp^{k.h}$$

$$u_w = u_o.\sin((k.x) + \omega)$$

$$v_w = u_o.\cos((k.x) + \omega)$$

Eqn. 1-3: Orbital motion calculations (Refer to Appendix C for further detail)

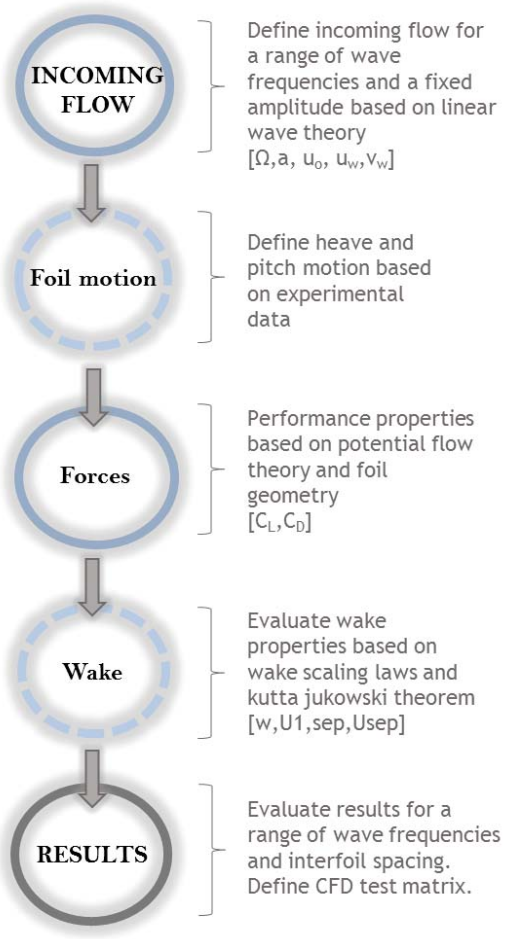

Fig. 4: Flow chart describing steps followed for the completion of the simplified numerical simulation

Foil heave and pitch motion is defined using sine functions representing the motion obtained during experimental testing. This allows for a more accurate representation of the motion of the foils when attached to the vessel.

Forward foil lift, flow separation points and velocity magnitudes are calculated by implementing the vortex sheet numerical method. The Kutta Jukowski theorem provides forward foil lift coefficient estimations *(Eqn.4)*. Furthermore, separation points and flow velocity magnitudes are presented in the form of contour flow plots.

$$C_L = \frac{L}{\frac{1}{2}\rho U^2 c} = -\frac{1}{c}\sum_{j=0}^{N-1} \tilde{\gamma}_j 2S_j$$

Eqn. 4: Kutta Jukowski lift coefficient calculation

Velocity magnitudes were evaluated at a given angle of attack, for an incoming uniform flow normalized to $|1|$.Thus, does not consider variations in flow direction as per wavy flow. However, scaling values in accordance to the incoming velocity at the specified foil angle of attack, will provide a valid estimate.

The variation of incoming velocity magnitude causes variations in Reynolds Number, which in turn affect drag values. Drag coefficient values were obtained with the use of XFOIL MIT. (2019) for a range of Reynolds number based on the maximum and minimum velocity obtained at any wave frequency.

Wake development was calculated based on Wake scaling laws, using the body thickness 'd' and flow speed 'U'. The coefficients are given for the 2D turbulent wake from

Schlichting, H. (1968 (9th Edition 2017)). It must be noted that Reynolds values lie within both laminar and turbulent range. However, both foils are mostly at high angles of attack. Thus, it was assumed that turbulent flow would be dominant. *Table 3,* shows the method used to calculate wake width and velocity defect, developing in the x-direction. *Fig.5* shows a diagrammatic representation of turbulent wake development.

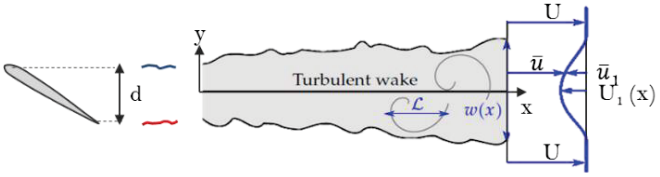

[4]

Fig.5: Wake development diagram

	w/d	U1/U
Laminar 2D	$\sim Re_x^{-1/2}(x/d)$	$\sim C_D(x/d)^{-1/2}$
Turbulent 2D	$\approx 0.57(C_D\, x/d)^{1/2}$	$\approx (C_D\, d/x)^{1/2}$

Table 3: Wake scaling laws

5.2 Results

Wake development trends show expected results. As the distance 'x' increases from the body, wake width increases. The contrary occurs when evaluating velocity defect, showing a decrease. Furthermore, plots also show minor differences as wave frequency is varied. *Graphs 1 & 2,* show results obtained.

Taking into account the location of the aft foil regarding forward foil wake, it can be seen that the further apart the foils are located the closer the flow encountered by the aft foil will be to the incoming flow. This draws attention to identifying at which interfoil spacing foil interaction can be considered negligible. Furthermore, the evaluation of velocity magnitude flow plots will provide insight on whether wave orbital velocity magnitudes overcome forward foil wake.

Maximum and minimum lift coefficient values were plotted, comparing both foils for a range of wave frequencies. There is a noticeable difference in forward and aft foil performance. This is due to the aft foil operating at lower angles of attack. Rising the question whether forcing the aft foil to oscillate at the same frequency and amplitude as the forward foil, could improve overall thrust. *Graph 3* shows the maximum and minimum lift coefficients for both foils.

Fig.6, shows a flow plot obtained for 14 deg. angle of attack. Providing a visual representation of the flow around the foil, along with separation points visible at the leading and trailing edge. A decrease in flow velocity is expected below the leading edge, followed by an increase above. A change in flow velocity is also expected at the trailing edge, though not shown at this stage of the analysis. This is due to the foil geometry entered having such a small thickness.

Research undertaken by Bowker, J. A. (2018) showed that maximum thrust was achieved at an interfoil spacing of 110% (1/2LWL from LCG), with a wave frequency of 4 rad. Results also showed that the foil motion was in phase with

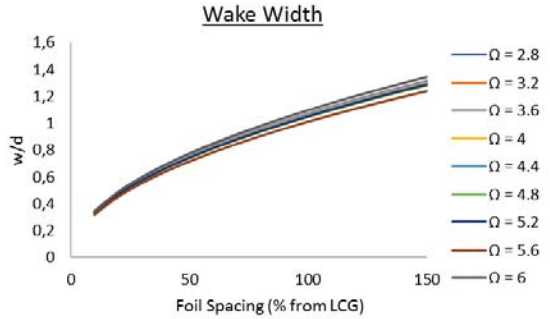

Graph 1: Forward foil wake width

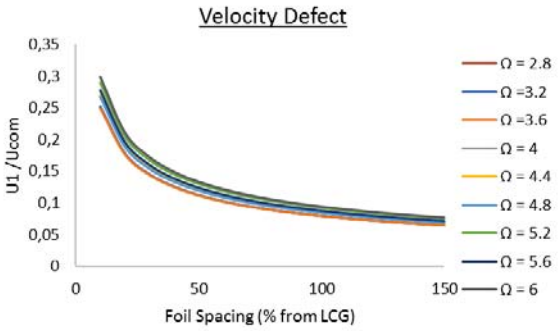

Graph 2: Forward foil wake velocity defect

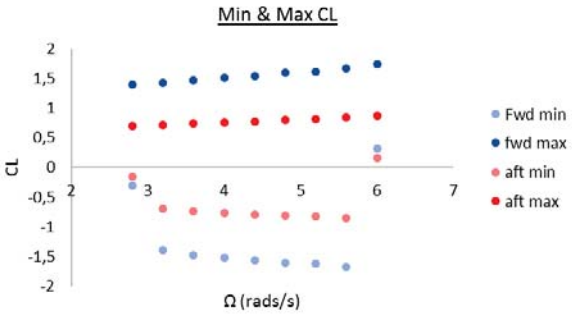

Graph 3: Max & min lift coefficients

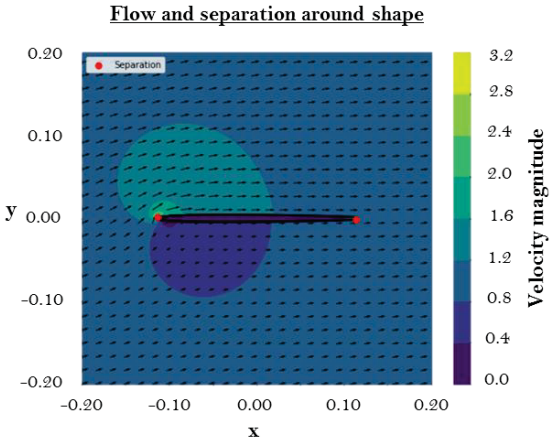

Fig.6: Normalized flow plot at maximum angle of attack

orbital motion at this location. *Graph 4,* shows a 3D plot of the velocity at the separation point, decreasing at the rate obtained evaluating wake velocity defect 'Uwake'. For a range of wave frequencies and interfoil spacings. *Graph 5*, shows a comparison of velocity magnitudes at a wave frequency of 4 rads.

Results show that an intersection occurs at approximately 100% (1/2LWL from LCG) interfoil spacing. Suggesting that foil interaction could be negligible at 100% (1/2LWL from LCG) interfoil spacing or higher.

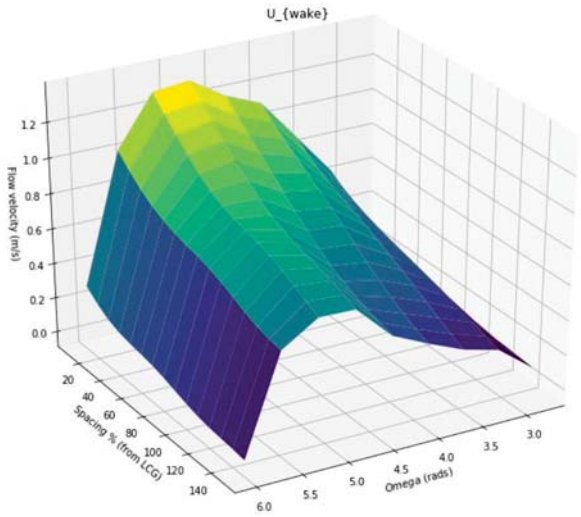

Graph 4: 3D U_{wake} plot at maximum angle of attack

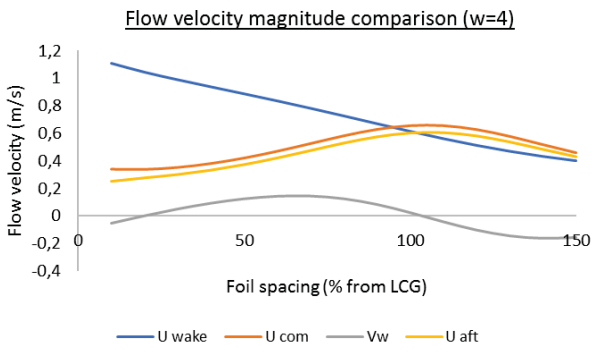

Graph 5: Flow velocity comparison at ω=4

This simplified numerical analysis has provided a useful tool to evaluate the hydrodynamic aspects of foil performance. Results obtained led to the definition of the test matrix followed during the computational fluid dynamic analysis. For further detail on the method used for the completion of the simplified numerical simulation, refer to Appendix C.

6. CFD SIMULATION

6.1 Introduction

The influence of wave orbital motion and foil interaction is further explored by carrying out CFD testing. It must be noted that the investigation was to be continued with the completion of towing tank testing of the Autonomous Vehicle 'Fleur', at University of Southampton facilities. This would have provided experimental data directly related to the problem analysed, and the possibility to compare results against previous runs. The use of CFD as an alternative method requires considerable computational power. Thus, resulting in a reduction in number of runs during the time available.

6.2 Validation

Prior to the analysis, the setup must be validated to ensure results obtained are accurate. Results were compared against experimental airfoil data by ABBOTT, I. H. (1959). The simulation was set to represent the experimental method carried out. Thus, a steady turbulent simulation was set at an equal Reynolds number of $3.0x10^6$, for an overset NACA0012 foil of 1m chord.

The analysis was run for a range of angles of attack, 0 to 6 deg. in intervals of 2 deg. Lift and drag coefficient values were compared against experimental data. *Graph 6 & 7*, show the comparison undertaken for lift and drag coefficient.

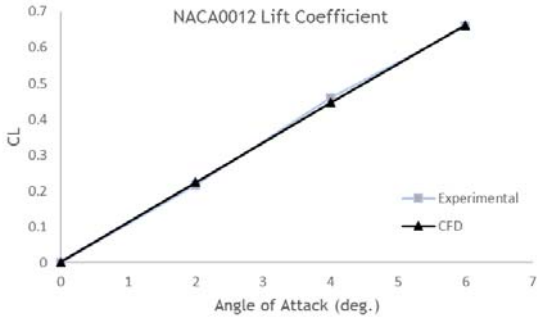

Graph 6: Lift coefficient validation

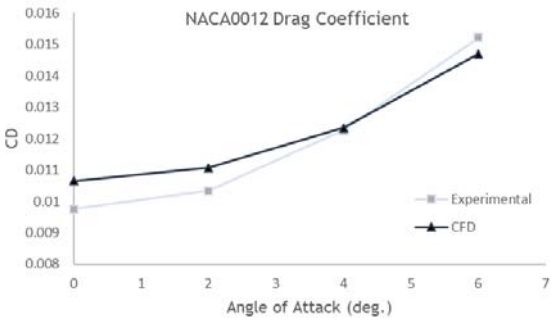

Graph 7: Drag coefficient validation

Furthermore, a mesh independence and time step study were carried out in order to identify the optimal setup, taking into account computational power and accuracy of results. *Graphs 8 & 9*, show the variation in lift coefficient percentage error. Where the optimal setup is marked in red.

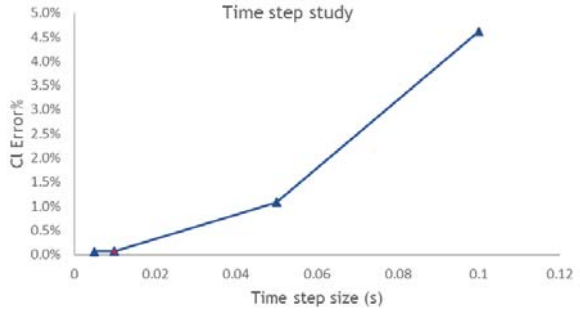

Graph 8: CL percentage error for varying time-step size

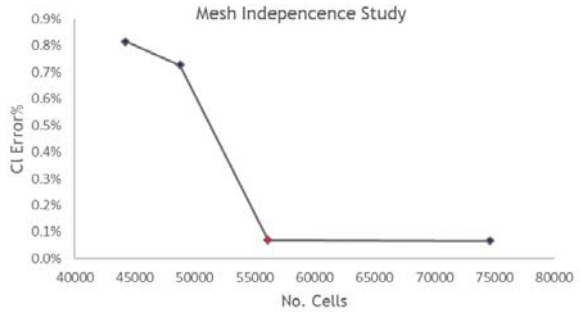

Graph 9: CL percentage error for varying mesh size

An optimal setup was identified, including a mesh composed of a total of 56110 cells and a time step size of 0.01s.

6.3 Setup

As described in Section 5, attention is drawn towards undertaking the analysis at a wave frequency of 4 radians. Thus, the study is continued with the use of CFD in order to analyse the resultant flow and forces further. Validating the proposed setup then led to the definition of the final method used to run each simulation. Key aspects of the methodology are summarized in *Table 4.* It must be noted that the setup described involves several assumptions and limitations listed below;

Assumptions:

- Deep water waves
- Small amplitude waves
- 2D Geometry
- Hull interaction negligible
- Foil pivot point at leading edge
- Constant fluid temperature

Limitations:

- Head waves
- Prescribed pitch and heave motion
- Doppler effect excluded
- Single fluid phase

Most limitations involved in the use of this method are set by the computational power available.

The geometry was modelled with the use of Ansys Fluent Design Modeler. The NACA0012 foil section was imported as a coordinate file and translated for a corresponding interfoil spacing. The mesh was then developed as three separate surfaces:

I. Background mesh
II. Forward foil mesh
III. Aft foil mesh

Forward and aft foil meshes were defined ensuring Y_{1+}>30.In order to avoid placing the centre of boundary-layer cells within the transitional region. Dynamic meshing was replaced by the use of overset meshing to define foil motion, conserving mesh refinements in critical areas. Once again reducing required computational power. *Fig.7.* shows the mesh setup, including a total of 56110 cells.

Geometry	
Foil type	NACA0012
Chord	0.23 m
Flow	
Wave frequency, Ω	4 rad
Wave amplitude	0.06 m
Variable	
Interfoil spacing (% from LCG)	50%,80%,110% &140%
Pitch motion	1. +/-14 deg. Both foils 2. Pitch angle obtained during experimental testing
Model	
	k-epsilon (2eqn) Realizable Standard wall functions
Solution	
	Scheme: Coupled Spatial discretization: Second order upwind Transient formulation: First order implicit
Run	
	Time steps: 1300 Time step size: 0.01s Iterations/step: 300
Outcome	
Inlet velocity magnitude plot Lift coefficient Drag Coefficient Force x-dir. Plot (Thrust) Velocity magnitude animations	

Table 4: CFD setup summary

A transient 2D RANS simulation was carried out for two foils in tandem configuration. The k-epsilon (2eqn) Realizable model was chosen, applying standard wall functions. Offering the same applications as k-epsilon RNG, additionally providing higher accuracy and easing convergence.

A constant seawater density at 15˚C of 1026.021 kg/m^3, in accordance with ITTC Conference, I. I. (2011) water properties was defined. Due to the involvement of wavy flow, flow velocity is dependent on time. Thus, Reynolds number is also a function of time, ranging from 5.61x10^4 to 1.24x10^5. Flow becomes turbulent at a range of 5x10^5 < Re < 3x10^6. Thus, the flow encountered is laminar. However, the foils are in motion and reach angles of attack exceeding 20 deg. Therefore, it is assumed that at such high angles of attack a turbulent simulation would represent this type of analysis more accurately.

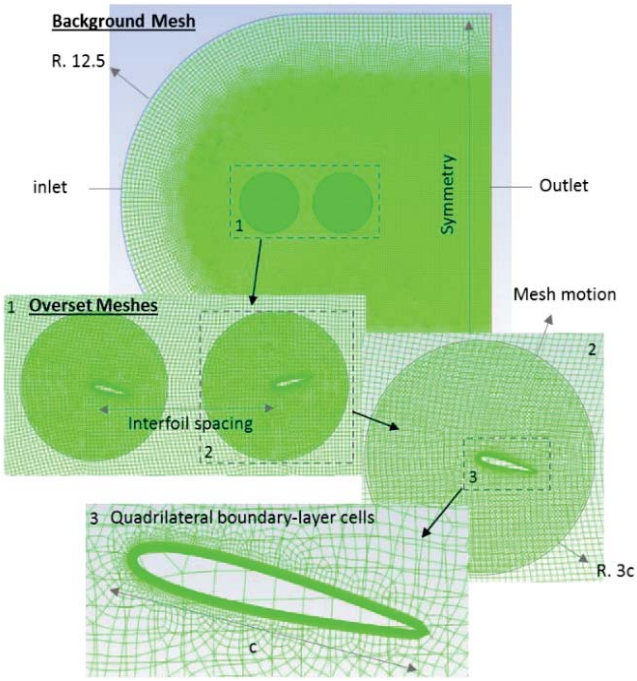

Fig.7: Overset mesh

$$IF\left((\sin\omega t) > 0, (\sin\omega t) + \left({}^{\alpha}/_{T_f} - (\sin\omega t)\right), (\sin\omega t) + \left(-{}^{\alpha}/_{T_f} - (\sin\omega t)\right)\right)$$

$$IF\left((\sin\omega t) > 0, (\sin\omega t) + \left({}^{h}/_{T_f} - (\sin\omega t)\right), (\sin\omega t) + \left(-{}^{h}/_{T_f} - (\sin\omega t)\right)\right)$$

Eqn. 5 & 6: Inlet velocity expressions for the x and y directions

To ensure the completion of this stage of the study, variables were reduced by running calculations for a fixed wave frequency. The inlet velocity is defined with the use of wave motion theory shown in *Eqn. 5 & 6*. Furthermore, defining the foils free to pitch and heave is complex and would once again require higher computational power. Thus, foil pitch and heave motions were prescribed.

Angles of attack expected for each foil at a given interfoil spacing were considered based on previous experimental data *(Table 5)*. Pitch pivot points were defined at each corresponding foil leading edge. A second set of runs was carried out with equal pitch motion for both foils in order to evaluate differences in foil performance if the foils were to actively pitch.

As shown in *Table 6*, a range of interfoil spacings from 50% to 140% in intervals of 30%, were evaluated. The simulation was run for 1300 time-steps, covering 13s (7 pitching cycles).

Foil pitch angles; Experimental Data

Spacing (m)	+/-0.6	+/-1.2	+/-1.8
Forward	~ 12°	~ 21°	~ 26°
Aft	~ 9°	~ 12°	~ 13°

Table 5: Pitch motion based on experimental data

s %	50%	80%	110%	140%
s (m)	≈0.57m	≈0.91m	≈1.25m	≈1.59m

Table 6: Range of interfoil spacing

6.4 Results

A first set of results were obtained prescribing forward and aft foil motion based on experimental data. Trends obtained show an increase in foil performance as foil pitch angle increases. Furthermore, aft foil performance is considerably lower in comparison to the forward foil. However, there is an increase in thrust generated by the aft foil as interfoil spacing increases. This could be due to a reduction in foil interaction effects.

Additionally, foil performance is also a function of wave phasing. As described by Yamaguchi, H., & Bose, N. (1994), the phase difference between the vertical velocity component of the wave orbital motion and the heave motion of the foil is a major factor in foil performance. The optimal wave phasing parameter occurs at π/2.

Experimental data by Bowker, J. A. (2018) shows that the optimal foil-wave interaction occurs at 110% interfoil spacing for the specified incoming wave frequency. As shown in *Graph 10*, maximum forward foil thrust is achieved at 110% interfoil spacing, coinciding with conclusions drawn by Bowker, J. A. (2018). Appendix B, describes the effect the wave phasing parameter has on vessel performance.

A second set of results were obtained evaluating foil performance for equal pitch motion at +/-14 deg. As shown in *Graph 11*, although both foils have equal prescribed motion, the forward foil generates higher

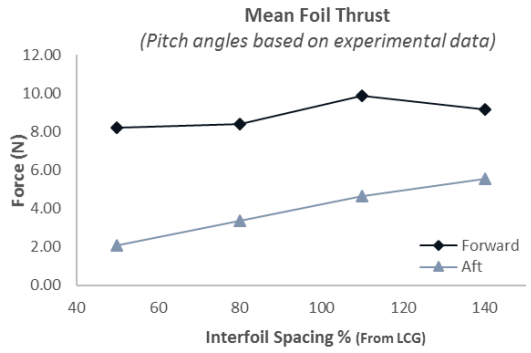

Graph 10: Mean foil thrust (pitch motion based on experimental data)

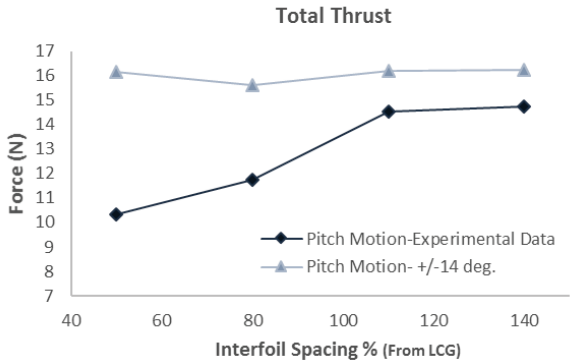

Graph 12: Total thrust

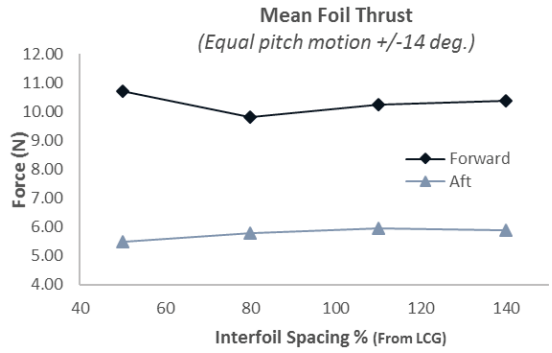

Graph 11: Mean foil thrust (Equal pitch motion +/-14 deg.)

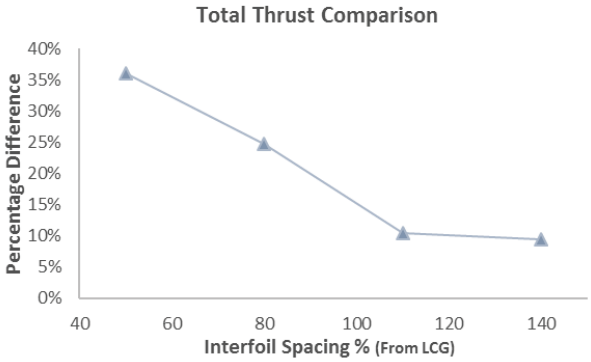

Graph 13: Total thrust comparison between methods

thrust. However, an increase in aft foil performance is obtained due to an increase in angle of attack. An estimated 30% increase in thrust can be obtained per 1 deg. increase in angle of attack.

The total thrust for both set of results were compared showing higher total thrust at 50% and 80% interfoil spacing. At 110% interfoil spacing the foil pitch angle is greater than 14 deg. Thus, a higher thrust is generated for prescribed pitch motion based on experimental data. At interfoil spacing greater than 100%, foil pitch angles exceed 20 deg. Suggesting that an increase in angle of attack at high interfoil spacing could cause stall and therefore a reduction in foil performance. *Graph 12*, shows the total thrust obtained for both sets. *Graph 13*, shows the percentage difference in total thrust generation between prescribed experimental pitch and equal pitch motion at +/- 14 deg.

Observations on the resultant flow were achieved with the inclusion of contour and vector plots. The resultant velocity magnitude was non-dimesionalized over the average inlet velocity vel_{mag}/vel_{inlet}. The objective of this section of the analysis is to provide insight on whether the wave orbital motion overcomes forward foil wake.

Evaluating if the aft foil encounters a vortex shed by the forward foil.

Observations commence at a time step in which the foils generate a large force. Therefore, causing vortex shedding. *Fig. 8 & 9* show an example at 1.3s, for interfoil spacings 50% and 110%. At 50%, foil interaction is clearly visible. Showing that wave orbital motion does not overcome forward foil wake. However, at 110% interfoil spacing, there is minimal foil interaction. The vortex shed by the forward foil is overcome by the wave orbital motion. Results obtained coincide with conclusions drawn in Section 5, with the use of simplified numerical methods.

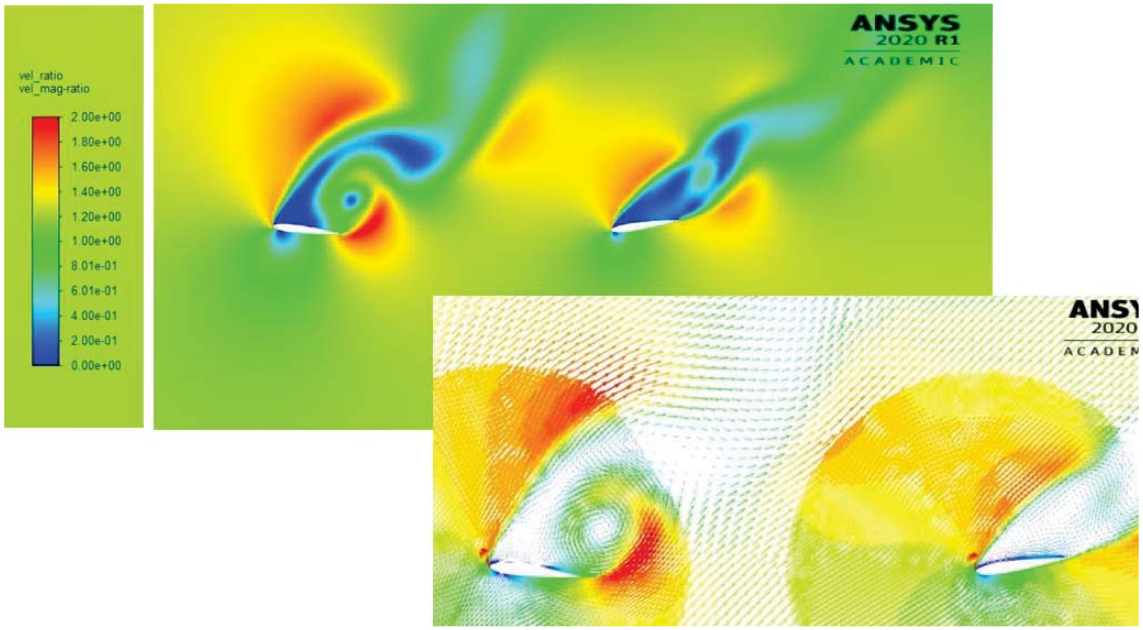

Fig.8: Contour and vector flow plot for 50% interfoil spacing, at 1.3s

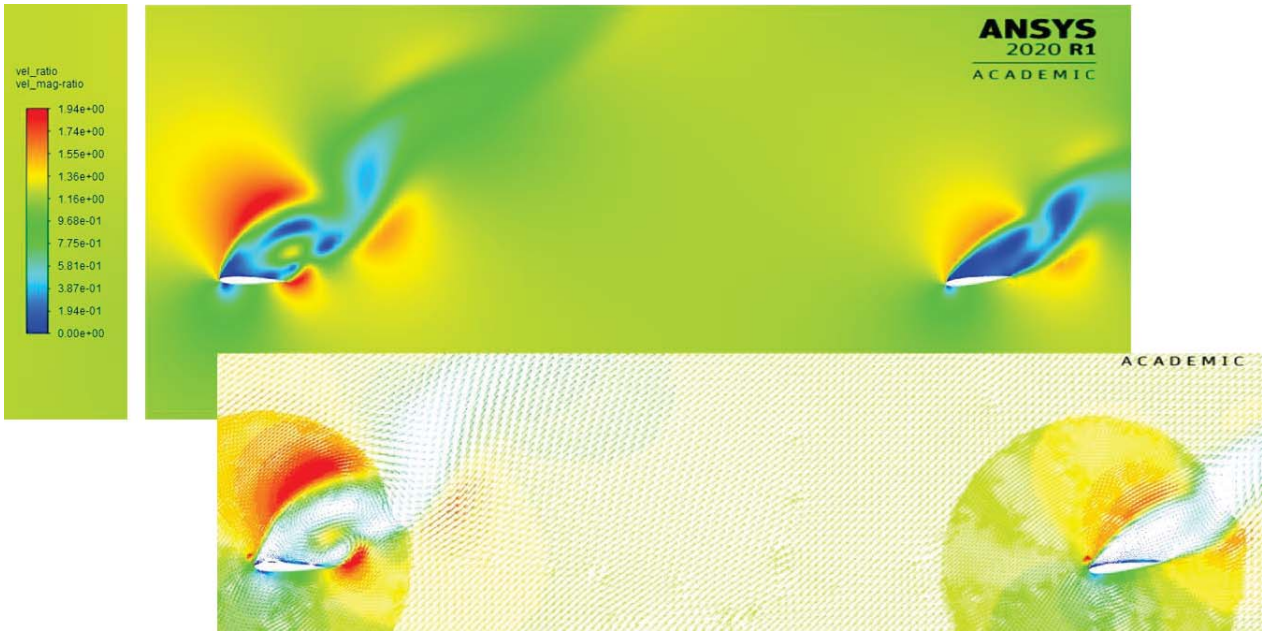

Fig.9: Contour and vector flow plot for 110% interfoil spacing, at 1.3s

Fig. 9, also suggests that an optimal interfoil spacing satisfying all flow components cannot be achieved at 110% interfoil spacing. The location of both foils provides an optimal interfoil spacing regarding vessel pitch motion and foil-wave interaction. However, it is highly improbable for an increase in aft foil performance to occur, due to an increase in velocity caused by a forward foil vortex. For further detail on the methodology and analysis of results, refer to Appendix D.

7. DISCUSSION

The study has been successfully completed providing data regarding the hydrodynamic aspects involved in the use of pitch induced flapping foils. The simplified numerical simulation undertaken provides a rapid tool to evaluate any symmetric NACA foil for a range of wave frequency. The methodology undertaken can be adapted for the study of foils in a variety of engineering research projects. Additionally, the validated mesh for use in Ansys Fluent can be adapted for any simulation of similar characteristics.

Results obtained coincide with previous publications. Additionally, contributing data on foil interaction and visual representations of the resultant combined flow. As described throughout the study, it is highly improbable to achieve a foil setup that satisfies optimal vessel pitch motion, optimal wave phasing and further improvement in foil performance due to foil interaction.

However, the completion of this analysis has provided enough data to undertake an evaluation on the effect of interfoil spacing on foil performance. Moreover, it can be concluded that foil interaction can be considered negligible with the use of an autonomous vehicle with interfoil spacing exceeding 100% $_{(1/2LWL\ from\ LCG)}$. Differences in foil performance passed 100% $_{(1/2LWL\ from\ LCG)}$ inerfoil spacing are due to foil-wave interaction effects. At interfoil spacings lower than 100% $_{(1/2LWL\ from\ LCG)}$, the total difference in foil performance is yet to be categorized between foil interaction and foil-wave interaction effects.

Furthermore, results obtained show that a considerable improvement in overall thrust can be achieved by increasing aft foil pitch motion. All aspects evaluated throughout the study require further work, described in detail in the upcoming section.

8.FURTHER WORK

The study undertaken requires further work in order to tackle the effects of all variables. Furthermore, the analysis involves numerous assumptions and limitations that affect results quantitatively and qualitatively. The following suggestions are provided on further work that could enhance the presented study:

- The completion of a 2D/3D CFD analysis with the above described setup. However, allowing for both foils to heave and pitch freely.
- The completion of a 3D CFD analysis on the full vessel arrangement. Thus, including vessel hull and foil rigid

arms. The purpose of the study being the evaluation of hull interaction.

- The completion of a 2D/3D CFD analysis with fixed interfoil spacing and wave frequency, for varying forward foil geometry. The purpose of the study being the evaluation of forward foil wake for varying foil geometry in wavy flow.
- The completion of experimental testing for the above described analysis.
- The completion of experimental testing for varying pitch motion. The purpose of the analysis being the evaluation of foil performance when actively pitching.

[5]

Fig.10: Experimental testing of an ASV 'Fleur' at University of Southampton facilities

Computational studies can be carried out with the use of Ansys Fluent ANSYS, I. A. (2020) as per the described analysis or alternatively Star-CCM+. On the other hand, experimental testing can be undertaken with the use of an ASV. Additionally, different foil geometries could be laminated in GRP/FRP or alternatively 3D printed. *Fig 10.* shows an image taken during experimental testing of an ASV in University of Southampton Towing Tank facilities.

9. REFERENCE

1994-2020 The MathWorks, I. (n.d.). MatLab Mathworks. 1994-2020 The MathWorks, Inc.

Katzmayr. (1922). 'Effect of Periodic Changes of Angle of Attack on Behaviour of Airfoils.' 20.

ABBOTT, I. H. (1959). Theory of Wing Sections. New York: DOVER PUBLICATIONS, INC.

ANSYS, I. A. rights reserved. (2020). Ansys Fluent. ANSYS, Inc. All rights reserved.

ANSYS, I. A. (2020). www.ansys.com. Retrieved from 2020 R1: https://www.ansys.com/about-ansys/get-in-touch

[8] Ansys.Inc. (2009, 01 29). www.afs.enea.it. Retrieved from Ansys Fluent: https://www.afs.enea.it/project/neptunius/docs/fluent/html/ug/node785.htm

Bøckmann, E. (2016). 'Wave Propulsion of Ships.' 01, 212.

[5] Bowker, J. A. (2018). 'Coupled Dynamics of a Flapping Foil Wave Powered Vessel.' 251.

[7] Clasen, J., Aranha, A. S., & Chipolina, A. (2020). Marine Hydrodynamics Coursework 3. Southampton: University of Southampton.

Copyright 2020 Anaconda, I. A. R. R. (n.d.). Anaconda. Copyright 2020 Anaconda, Inc. All Rights Reserved.

Conference, I. I. (2011). ITTC – Recommended Procedure; Fresh Water and Seawater Properties. ITTC Specialist Committee on Uncertainty Analysis.

De Silva, L. W. A., & Yamaguchi, H. (2012). 'Numerical study on active wave devouring propulsion.' Journal of Marine Science and Technology (Japan), 17(3), 261–275.

Epps, B. P., Muscutt, L. E., Roesler, B. T., Weymouth, G. D., & Ganapathisubramani, B. (2017). 'On the interfoil spacing and phase lag of tandem flapping foil propulsors.' Journal of Ship Production and Design, 33(4), 276–282.

[3]Gauthier, M., & John's Newfoundland, S. (2018). 'Wave-Assisted Propulsion for Autonomous Surface Vehicles.' May.

I.E.Garrick. (1936).' Propulsion of a Flapping and Oscillating Airfoil.' 14.

Inc, A. (2020). www.anaconda.com. Retrieved from Python 3.7: https://www.anaconda.com/products/individual

Jones, K. D., Dohring, C. M., & Platzer, M. F. (1998).' Experimental and computational investigation of the Knoller-Betz effect.' AIAA Journal, 36(7), 1240–1246.

[2] Kaplan, P., & Hugli, W. C. (1954). 'The Two-Dimensional Wake and Downwash of a Hydrofoil in Waves.' 19.

[1] Kinsey, T., & Dumas, G. (2012). 'Optimal tandem configuration for oscillating-foils hydrokinetic turbine.' Journal of Fluids Engineering, Transactions of the ASME, 134(3).

Lighthill, J. (1975) ‘Mathematical Biofluiddynamics’, Society for Industrial and Applied Mathematics.

MIT. (2019). web.mit.edu. Retrieved from XFOIL6.99: https://web.mit.edu/drela/Public/web/xfoil/

Muscutt, L. E., Weymouth, G. D., & Ganapathisubramani, B. (2017). Performance augmentation mechanism of in-line tandem flapping foils. *Journal of Fluid Mechanics*, *827*, 484–505.

Muscutt, L. E., Dyke, G., Weymouth, G. D., Naish, D., Palmer, C., & Ganapathisubramani, B. (2017). ‘The four-flipper swimming method of plesiosaurs enabled efficient and effective locomotion.’ Proceedings of the Royal Society B: Biological Sciences, 284(1861), 6–11.

Parsons, C. (1914). ‘Propulsion of Ships.’ In Journal of the American Society for Naval Engineers (Vol. 26, Issue 1).

Schlichting, H. (1968 (9th Edition 2017)). Boundary Layer Theory. Berlin: Springer Nature.

Theodorsen, T. (1949). ‘The General Theory of Aerodynamic Instability and the Mechanism of Flutter.’ 26.

Wang, Q., Ma, P., & Xie, Y. (2019). ‘Effect of foil thickness on the hydrodynamic behavior of a self-sustained oscillating foil system.’ ACM International Conference Proceeding Series, November, 127–131.

[6] Weymouth, G., & Southampton, U. o. (2020, 03). Hydrodynamics Python Code Files_Vortex Panel Method. Southampton, Hampshire, UK.

[4] Weymouth, G., & Southampton, U. o. (2020). Notes on Marine Hydrodynamics. Southampton: University of Southampton.

Yamaguchi, H., & Bose, N. (1994). ‘Oscillating foils for marine propulsion.’ Proceedings of the International Offshore and Polar Engineering Conference, 3(July), 539–544.

A.APPENDIX- Literature Review

Publication	Study	Significant Parameters	Factors not considered
Yamaguchi, H.(2012)	Optimal wave phase difference of a single 2D oscillating foil in wavy flow.	$\Psi = \Pi\ (\Omega, a, Fr)$	-Interfoil spacing -Forward foil wake
Epps, B. P. (2017)	Foil interaction and optimal phase lag of foils in tandem.	$\Phi_{opt} = \Pi\ (s, \Phi_0, U^*, U, U\tau)$	-Wave orbital motion
Hugli, W. C. (1954)	Change in aft foil angle of attack based on wake and downwash of a single 2D Hydrofoil in Waves.	$\Delta a = \Pi\ (s, \Omega, \varepsilon, U_{x,y\ wave/vortex})$	-Total thrust -Wave phase difference
Bowker, J. A. (2018).	Coupled Dynamics of a Flapping Foil Wave Powered Vessel.	$V = \Pi\ (s, \Omega, \Psi, h_i, \Theta_i)$	-Foil interaction

Where:
Ω - Wave frequency
a - Wave amplitude
Fr - Froude number
s - Interfoil spacing
Φ_0 *- phase offset*
U - a representative vortex advection velocity*

Uτ- vortex advection distance during one full flapping period
ε - downwash angle
$U_{x,y\ wave/vortex}$ *- magnitude of the wave orbital motion /magnitude of the vortex*
V - Forward vessel speed
h_i *- foil heave*
Θ_i *- foil pitch*

Table 7: Detailed literature review summary

B.APPENDIX- Wave Phasing Parameter

The wave phasing parameter relates the wave vertical velocity component with foil heave displacement. An optimal foil-wave interaction occurs when the wave and heave motion are totally off phase. Thus, as the foil heaves in a positive y-direction, the wave vertical component occurs in the negative y-direction. The optimal wave parameter results in π/2.

Bowker, J. A. (2018) investigated the effect on wave parameter for a range of interfoil spacings and wave frequencies. It was found that the optimal foil-wave interaction would occur at 90%, 110% and 150% interfoil spacing. For a wave frequency of 0.8 Hz, 0.7Hz and 0.6Hz respectively. Experimental data obtained by Bowker, J. A. (2018) is shown in *Graph 14*. Furthermore, *Graph 15* shows maximum thrust was obtained at a wave parameter of π/2.

As the vessel encounters the incoming wave, the forward foil motion is purely dictated by the wavy flow. Whereas, aft foil motion is strictly dependent on vessel motion. Thus, having an optimal foil-wave interaction for both foils is improbable. However, aft foil performance could be improved by modifying the pitch motion.

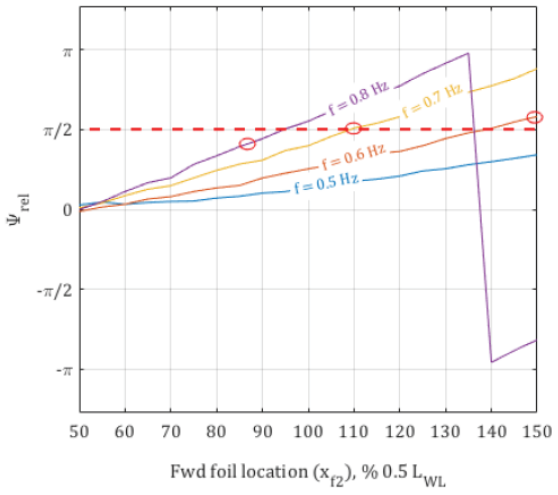

[5]

Graph 14: Wave phasing parameter by Bowker, J. A. (2018

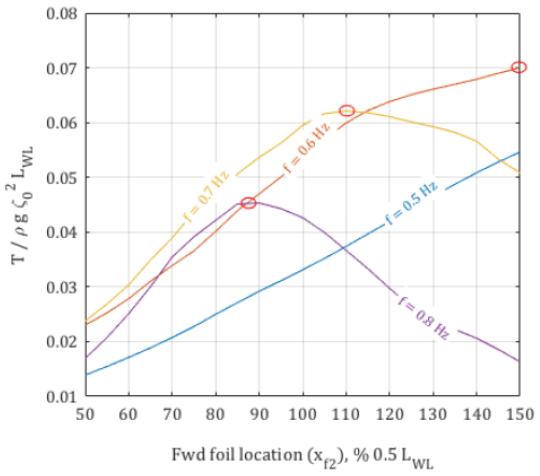

[5]

Graph 15: Non-dimensionalized thrust coefficient Bowker, J. A. (2018)

C.APPENDIX- Simplified numerical simulation

C.1 Combined Flow

To begin the theoretical analysis, the flow was defined. An incoming linear head wave was established requiring a single input, wave frequency, 'ω'. Wave particles adopt an oscillatory motion which results in an x and y velocity component. Wavy flow was defined as regular deep-water waves. Thus, velocity magnitudes vary as the wave travels in the x-direction and decreases as depth increases.

This results in the encountered flow being a function of foil location and distance travelled by the vessel. Including a mean forward vessel speed of 0.47 m/s, based on experimental data. *Table 8,* shows the method followed for the definition of wavy flow. *Graph 16,* shows the amplitude of the wave-induced fluid particle velocity against foil heave, for a range of wave frequency. Showing a decrease in velocity as depth increases. *Graph 17,* represents vessel forward speed against wave frequency, obtained from experimental data. *Graph 18,* shows the combined horizontal flow component for a range of wave frequencies.

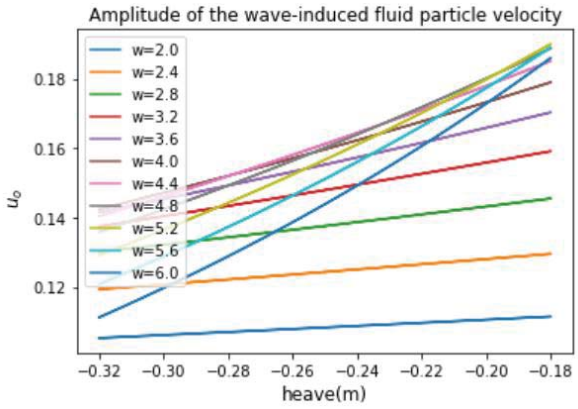

Graph 16: Amplitude of wave-induced fluid particle velocity

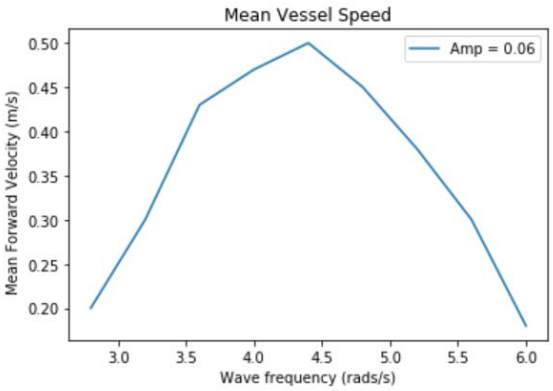

Graph 17: Mean vessel velocity based on experimental data

$$y = -5.t.c.\left(0.2969.\left(\frac{x}{c}\right)^{0.5} + (-0.126).\frac{x}{c} + (-0.3516).\left(\frac{x}{c}\right)^{2} + 0.2843.\left(\frac{x}{c}\right)^{3} + (-0.1015).\left(\frac{x}{c}\right)^{4}\right)$$

Eqn. 7: Thickness function for a NACA 4-Digit foil section

Wave Orbital Motion Calculations		
Amplitude of the wave-induced fluid particle velocity	$u_o = \frac{gka}{\omega}.exp^{k.h}$	$wavenumber = k = \frac{\omega^2}{g}$ $wave\ amplitude = \ a = 0.06$ $g = 9.81$ $frequency = \ \omega = 4$ $heave = \ h = \ \sin(\omega.t).\frac{y}{2} + 1.5.y$ $height = \ y = (-0.0159.\omega) - 0.11$
Horizontal and vertical components of fluid velocities	$u_w = u_o.\sin((k.x) + \omega)$ $v_w = u_o.\cos((k.x) + \omega)$	$x = distance\ travelled\ in\ x - dir$ Dependant on time thus 'x' represented as time step 't'

Thus combining equations the final inlet velocity expressions x-dir and y-dir:

$$\boldsymbol{u_w = \frac{gka}{\omega}.exp^{k\sin(\omega.t).\frac{y}{2}+1.5.y.}.\sin((k.t)+\omega)}$$

$$\boldsymbol{v_w = \frac{gka}{\omega}.exp^{k\sin(\omega.t).\frac{y}{2}+1.5.y.}.\cos((k.t)+\omega)}$$

Table 8: Wave orbital motion calculation method

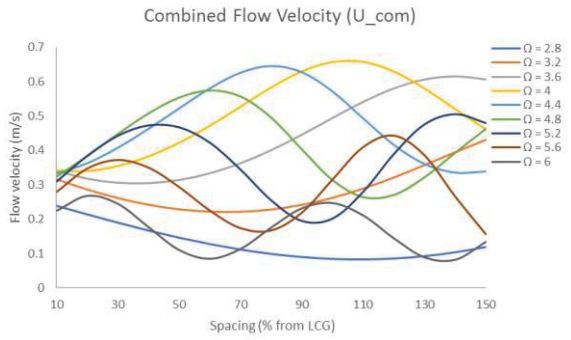

Graph 18: Combined flow velocity U_{com}

C.2 Foil Motion

As the flow is defined, the vessel motion is obtained. The foils heave and pitch as a function of vessel pitch motion, which in-turn is a function of wave frequency. Data obtained during experimental testing by Bowker, J. A. (2018), show forward and aft foil response plots where heave and pitch amplitudes are obtained. This was simplified as a sinusoidal function.

As the foils are in motion, there is a variation in flow velocity and therefore Reynolds number. This results in an oscillatory lift and drag coefficient per foil, as a function of time. Drag coefficient values were evaluated with the use of XFOIL MIT. (2019) for a range of Reynolds numbers, from minimum to maximum flow velocity encountered. Furthermore, a range of angle of attack +/- 14 deg. in intervals of 1 deg. were evaluated. *Graph 19*, shows forward foil drag coefficient values for a range of wave frequencies as the vessel travels in the x-direction.

C.3 Wake Development

Forward foil wake width and velocity defect was then estimated with the use of wake scaling laws, based on turbulent boundary layer theory. The theory relates to uniform flow, therefore results obtained are assuming the flow encountered is uniform at a specific instance in time. *Graph 20*, shows forward

foil wake width at maximum angle of attack for a specified wave frequency, non-dimensionalized by the body diameter. *Graph 21,* shows forward foil wake maximum velocity defect (occurring at y=0).

C.4 Vortex Panel Method

The analysis was continued using the vortex panel method.[6] Boundary layer decomposition is applied to the foil. The geometry is divided into a finite number of vortex panels discretizing the specified shape *(Graph 22)*. This allows for the definition of a geometry for which potential flow theory can be applied.[7] In order to define the foil shape, the thickness function for NACA 4-Digit Airfoil is used *(Eqn. 7)*.

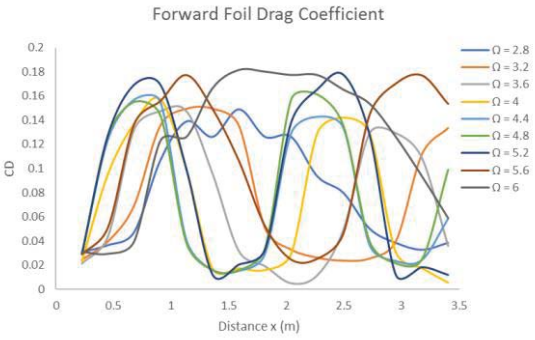

Graph 21: Forward foil drag coefficient

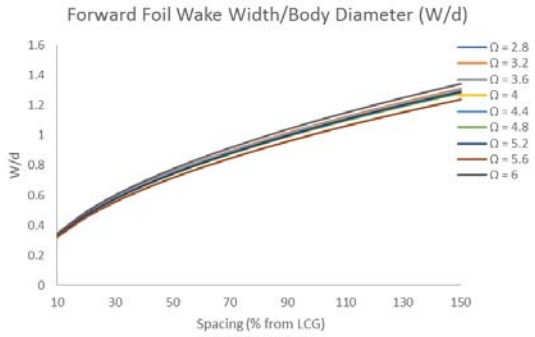

Graph 22: Forward foil wake width/body diameter (W/d)

The code carried out includes the possibility to refine the geometry at the leading and trailing edge by including a bias factor along with increasing the number of panels. Furthermore, a percentage truncation can be included for thin geometries if necessary, easing further calculations.

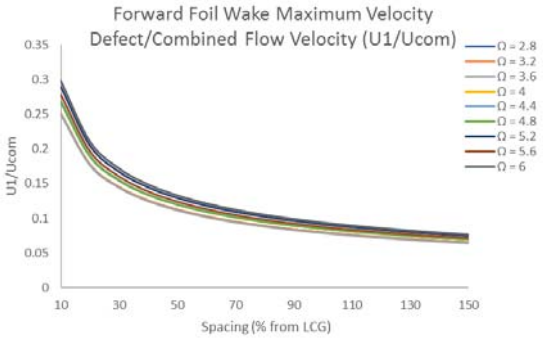

Graph 19: Forward foil wake maximum velocity defect/combined flow velocity ($U1/U_{com}$)

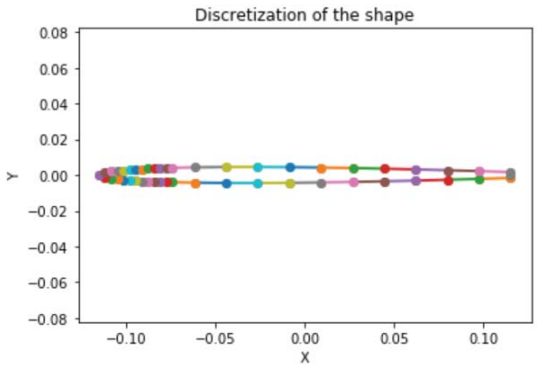

Graph 20: Foil discretization (geometry)

'All calculations are previously defined as functions, producing a set of analytical methods that can then be used and adapted for any application. All requiring the use of built-in functions and the implementation of hydrodynamic theory. For instance, solving the flow around a shape, depends on the evaluation of vortex strength on a defined PanelArray. Implementing this for a foil, an

additional kutta condition needs to be used, as described below. Furthermore, the identification of separation points refers to Thwaites' method providing a prediction on boundary layer separation.' [7]

The flow is solved with the use of two different kutta conditions, dependent on whether the foil is truncated. A non-truncated foil requires the kutta condition applied at the last two panels forming the tailing edge. In the case of a truncated foil, the condition is applied at the adjacent panels to the truncation. Thus, the side panels prior to the truncation. This is due to the kutta condition having to be located at the point of flow separation. Additionally, the function 'solve.gamma_O2', solves for the panel vortex strength. It is a second order method, linearly varied improving accuracy of results. [7]

Flow plots were then obtained for a range of angles of attack. Providing visual representations of normalized velocity magnitudes and separation points. *Fig. 11 to 14* show flow plots obtained for a range of angle of attack 0 to 12 deg. in intervals of 4 deg. Clearly showing an increase in velocity magnitude. Furthermore, an increase in pressure occurs at the stagnation point causing flow separation past this point along with a velocity defect. A vortex is expected at the leading and trailing edge of the foils.

Forward foil wake flow velocity was evaluated assuming the maximum occurs at the point of flow separation. Thus, wake velocity defect was deducted from the flow

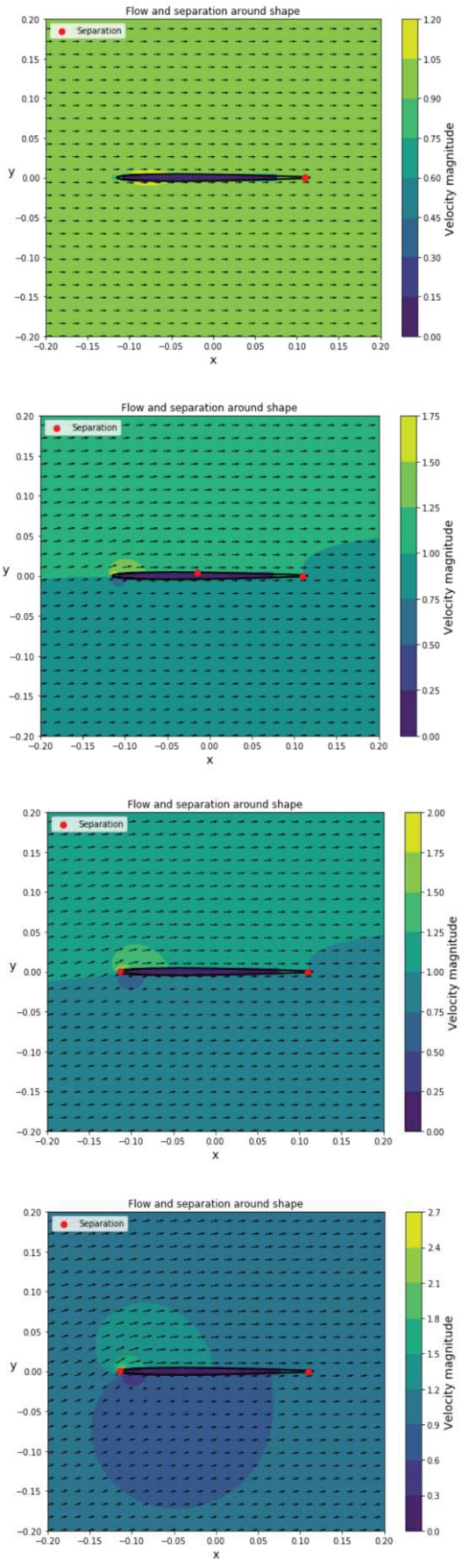

Fig.11 to 14: Normalized flow plots of the forward foil at 0,4,8 & 12 deg. respectively

velocity at separation 'U_{sep}', as a function of angle of attack and distance 'x'. This flow was represented as 'U_{wake}', shown in *Graph 23*.

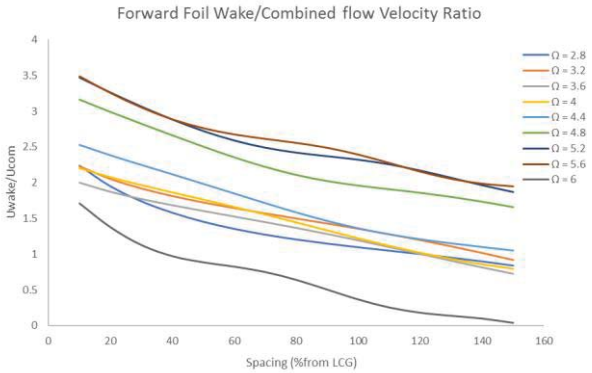

Graph 23: Forward foil wake/combined flow velocity ratio

Additionally, deducting the velocity defect to the combined incoming flow provides insight on the distance 'x' or interfoil spacing required for the aft foil to encounter an equal flow to that of the forward foil. *Graph 24,* plots 'U_{aft}' over 'U_{com}', showing both flow components reaching similar magnitudes at approximately 110% interfoil spacing.

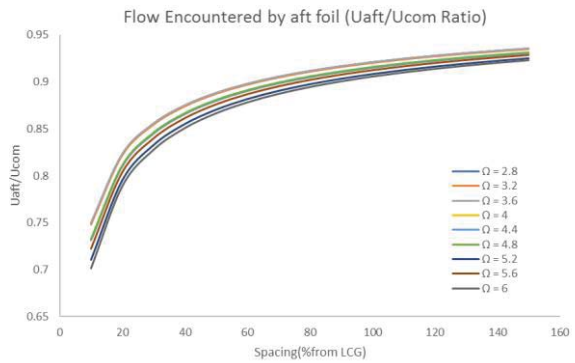

Graph 24: Flow encountered by the aft foil (U_{aft}/U_{com} Ratio)

C.5 Verification

The functions used throughout the process were verified against the solution obtained for a circle. A simple geometry such as a circle provides the possibility to compare against analytical results. The comparison was carried out for flow plot solutions and separation points. Furthermore, the lift coefficient has also been provided and validated against an analytic NACA0012 Cl solution. Plots have been obtained comparing numerical and analytical solutions. [7]

Graph 25 & Fig. 15, show the circular geometry defined and the normalized flow plot obtained. Including flow separation points. *Graph 26,* shows numerical results for panel vortex strength compared against analytical results. *Graph 27,* includes a comparison of lift coefficient values obtained numerically and analytically. Including values obtained with the use of XFOIL MIT. (2019).

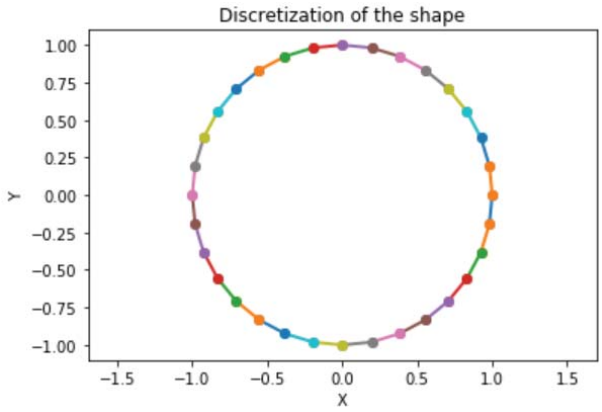

Graph 25: Discretization of the circular shape (geometry)

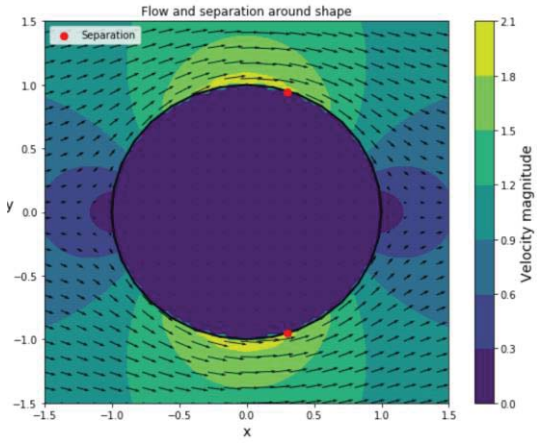

Fig.15: Normalized flow plot verification

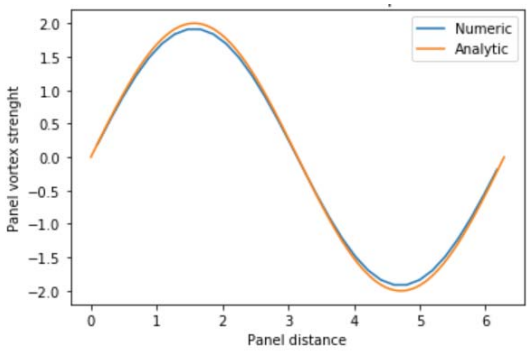

Graph 26: Foil lift coefficient verification

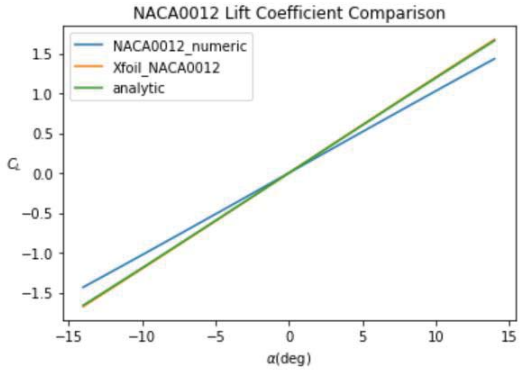

Graph 27: Panel vortex strength verification

D.APPENDIX- CFD

D.1 Validation

Simulation	No. Foils	Geom chord	Type	Overset	Heave	Y+	Y1 (mm)	U (m/s)	rho (kg/m3)	mhu (Pa.s)	Re
1-4	1	1	Steady	YES	NO	>30	1	43.82	1.225	1.79E-05	3.00E+06

No.	file name	alpha	ux (m/s)	uy(m/s)	Cl (exp)	Cd (exp)	Cl	Error%	Cd	Error%
1	sim_val_001	0	43.82	0.00	0.000	0.010	0.002	0.2%	0.011	9.2%
2	sim_val_002	2	43.80	1.53	0.217	0.010	0.224	3.3%	0.011	7.0%
3	sim_val_003	4	43.72	3.06	0.460	0.012	0.446	3.0%	0.012	0.6%
4	sim_val_004	6	43.58	4.58	0.659	0.015	0.662	0.5%	0.015	3.4%

Table 9: CFD validation- single fixed foil

Simulation	No. Foils	Geom chord	Type	Overset	Heave	Y+	Y1 (mm)	U (m/s)	rho (kg/m3)	mhu (Pa.s)	Re
5	2	1	Transient	YES	NO	>30	1	43.82	1.225	1.79E-05	3.00E+06

No.	file name	alpha	ux (m/s)	uy(m/s)	Cl (exp)	Cd (exp)	Cl	Error%
5	sim_val_2F_02	+/-14	43.82	0	0.000	0.010	0.009	1.0%
					0.217	0.010	0.227	4.6%
					0.460	0.012	0.462	0.6%
					0.659	0.015	0.675	2.4%

Table 10: CFD validation- single foil including prescribed pitch motion

No.	file name	Iter/time step	No. Time steps	Time step size (s)	No. Cells	Cl_fwd	Cl_aft	Cl Error %
6	sim_mesh_01	300	500	0.01	44239	1.464	1.387	0.8%
7	sim_mesh_02	300	500	0.01	48771	1.465	1.393	0.7%
8	sim_mesh_03	300	500	0.01	56110	1.475	1.395	0.1%
9	sim_mesh_04	300	500	0.01	74623	1.475	1.395	0.1%

Table 9: Mesh independence study

No.	file name	Iter/time step	No. Time steps	Time step size (s)	Cl_fwd	Cl_aft	Cl Error %
10	sim_time_01	300	500	0.1	1.544	1.118	4.6%
11	sim_time_02	300	500	0.05	1.460	1.448	1.1%
12	sim_time_03	300	500	0.01	1.475	1.395	0.1%
13	sim_time_04	300	500	0.005	1.475	1.352	0.1%

Table 10: Time-step independence study

D.2 Mesh

The mesh was set as an all quad arrangement, with an inflation both at the center of the background surface and around the foils. Edge sizing was applied for both foils for a total of 200 divisions per foil. A maximum cell size of 0.1m defines the background mesh, including a growth rate of 1.05. Additionally, the forward and aft overset meshes apply a maximum cell size of 0.05m with an equal growth rate.

$$Re_x = \frac{\rho . U . c}{\mu}$$ *Eqn. 8: Reynolds number*

$$c_f = \frac{0.027}{Re_x^{1/7}}$$ *Eqn. 9: Turbulent friction coefficient*

$$C_F = \frac{7}{6} c_f(L)$$ *Eqn.10: Total friction coefficient*

$$u^* = \sqrt{\frac{\tau_w}{\rho}}$$ *Eqn.11: Friction velocity*

$$\tau_w = \frac{1}{2} . \rho . U^2 . c_f$$ *Eqn.12: Wall shear stress*

$$Y_+ = \frac{u_\tau}{\nu} Y_1$$ *Eqn.13: Wall Y-plus*

Boundary layer meshing was defined based on flat plate theory. The minimum boundary layer cell size is found by specifying a desired 'Y_+' value. The main objective being the refinement of critical sections and consequently the positioning of cells in the turbulent or laminar region. Locating the centre of a boundary layer cell at the transitional region could cause inaccuracy of results. Eqn. 8 to 13, show flat plate theory calculations for the definition of boundary layer cell height 'Y_1'.

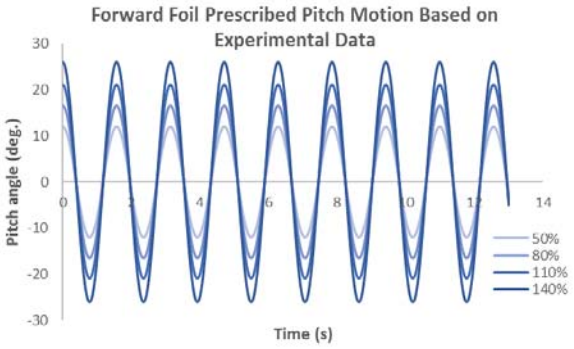

Graph 28: Forward foil pitch motion

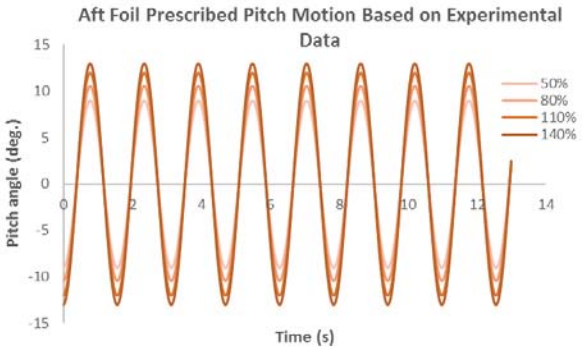

Graph 29: Aft foil pitch motion

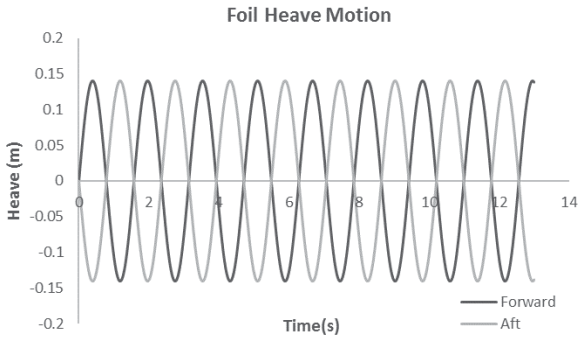

Graph 30: Foil heave motion

D.3 Setup

The heave and pitch motion prescribed based on experimental data was represented as sinusoidal functions. *Graphs 28 & 29,* show the forward and aft pitch motion. *Graph 30,* shows the heave motion prescribed for both foils.

Furthermore, the coupled solver was chosen regarding recommendations provided by experienced computational fluid dynamics engineers. As stated by Ansys.Inc. (2009, 01 29); 'Turbulent flow pressure-based solvers can be solved in a segregated or coupled manner. The coupled algorithm solves the momentum and pressure-based continuity equations together. An implicit discretization of pressure gradient terms allows for the full implicit coupling.' [8] Providing a suitable solver for an overset mesh setup.

D.4 Results

Convergence of solutions obtained is evaluated prior to the simulation by the completion of a validation, as described in Section 6. In addition, for each simulation run, monitoring residuals is also of importance. Residuals criteria was set at 1e-5, setting a boundary where valid results must lie below this limit. Results obtained show residuals lie between 1e-5 and 1e-12, continuity being the hardest residual to converge.

The methodology behind the evaluation of thrust within Ansys Fluent is based on the evaluation of lift and drag coefficients as a function of angle of attack and Reynolds number. *Eqn. 14 & 15* show the calculation undertaken by the software.

$$C_T = [C_{L\alpha}.\alpha.\sin\alpha] - [C_D(\alpha, Re).\cos\alpha]$$

$$T = \frac{1}{2}.\rho.c.U^2.C_T$$

Where:

$C_{L\alpha}$ = *Lift coefficient slope NACA0012*

α = *Foil pitch angle*

$U = U_{com}$ = *Combined flow*

Eqn. 14 & 15: Foil thrust coefficient & thrust force calculation

The final thrust plots provided in Section 6, are a result of a filtering process carried out on raw data obtained. The oscillatory nature of the propulsion system specified causes positive and negative forces in the x-direction. Therefore, each foil encounters thrust and drag. However, averaging these values should result in an overall thrust in order to propel the vessel forward.

Due to numerical instabilities, at points where the rotation of the overset meshes change direction, a high positive or negative peak force is encountered. These data points are filtered to ensure anomalies are neglected when completing averaging calculations. *Graphs 32 to 39,* show the raw data (not filtered) for both sets of runs. All plots show a clear trend and a common instant in time in which anomalous data occurs. For future reference if enough computational power is available, this error

could be avoided by setting the foils free to pitch and heave.

It must be noted that a 2D analysis will tend to overestimate foil performance. *Graph 31,* shows the overall thrust obtained during experimental testing by Bowker, J. A. (2018). Approximately 6.5N of average thrust were obtained at 0.7 Hz and a wave amplitude of 0.06m. The foils were located at forward and aft perpendiculars (100% interfoil spacing). An average thrust of 9.9N was achieved for 110% interfoil spacing with the use of CFD. This value is expected to decrease as per experimental data obtained by Bowker, J. A. (2018) if further experimental testing is to be carried out.

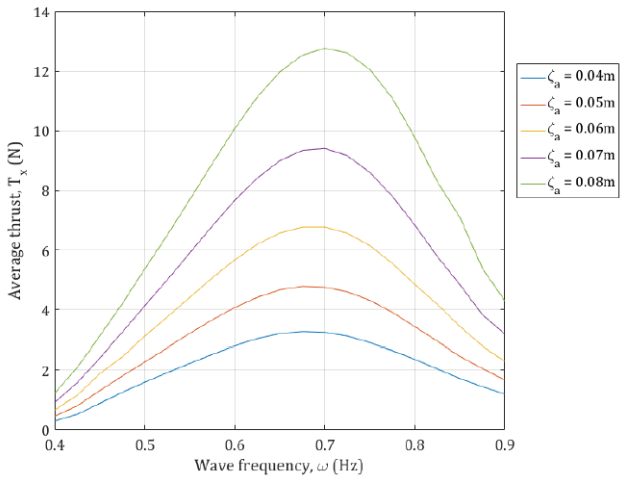

[5]

Graph 31: Average thrust by Bowker, J. A. (2018)

A vital component evaluated in this analysis is observations of the flow development at different time steps and interfoil spacings. Visual representations of flow velocity magnitude were obtained as contour plots and vector plots. The velocity was non-dimensionalized over the average inlet velocity, represented as $^{vel_{mag}}/_{\overline{vel_{inlet}}}$ .This allowed for the following evaluation:

- Flow velocity magnitude and direction for a full pitching cycle.
- Flow velocity magnitude and direction for a full incoming wave cycle.
- Foil interaction for a range of interfoil spacings.

The analysis begins with a collection of contour plots for 50% interfoil spacing. Where the pitch motion is prescribed at +/-14 deg., providing images of a full pitch cycle at time steps 40 to 200 *(Fig. 16 to 20)*. Within this cycle, it is noticed that the maximum inlet velocity occurs at 2.0s. However, the foils are at 0 deg. angle of attack and are not off phase from the incoming wave and therefore do not generate much thrust.

Additionally, at 0.8s the foils are also at 0 deg. angle of attack. At this time step the maximum inlet velocity is not encountered. However, the direction of the wave orbital motion is favorable resulting in high thrust generation. These observations are visible at all interfoil spacings. As shown in *Fig. 21 to 25,* at 140% interfoil spacing there is a decrease in foil interaction. A velocity defect in forward foil wake is noticeable decreasing incoming flow disturbance.

Similar evaluations were carried out for a full wave cycle, providing insight on wave orbital velocity magnitude and direction. The vector plots provided for 50% and 140% interfoil spacing *(Fig. 26 to 35)* clearly show the

variation in flow direction of the incoming wave. Additionally, alterations in flow direction due to vortex shedding at the leading and trailing edge of each foil is visible.

The incoming flow does not overcome forward foil wake at any time step of the wave cycle at an interfoil spacing of 50%. Meanwhile at 140% interfoil spacing, forward foil wake encounters a defect, decreasing wake velocity magnitude. Foil interaction is considered minimal.

Contour and vector plots at maximum and minimum inlet velocity, for a range of interoil spacing are shown in *Fig. 36 to 51.* Trends previously described are clearly visible varying timestep and interfoil spacing.

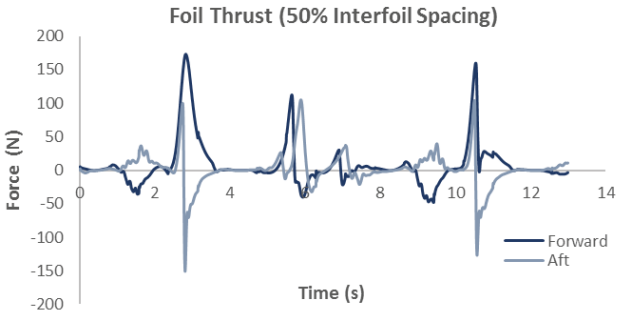

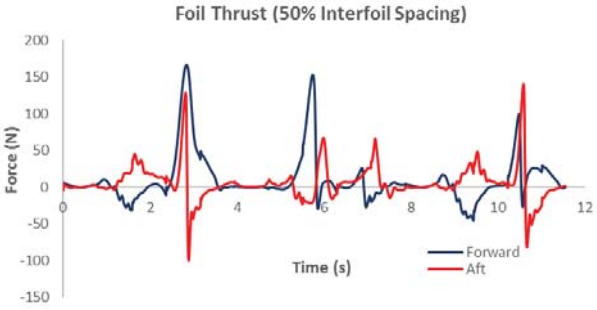

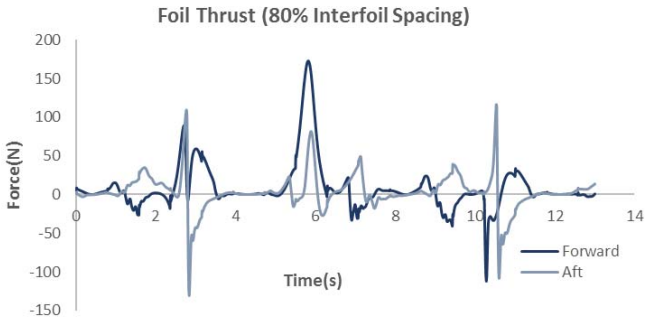

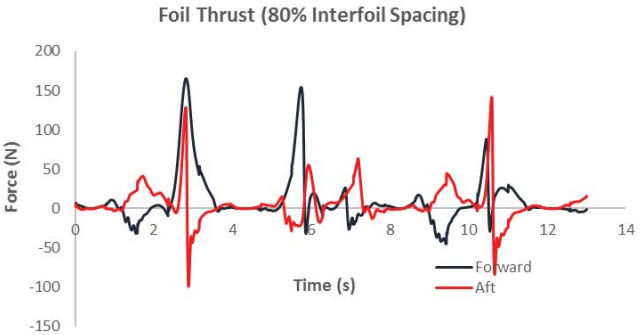

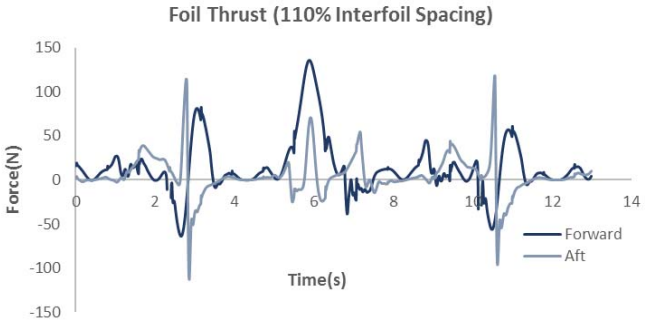

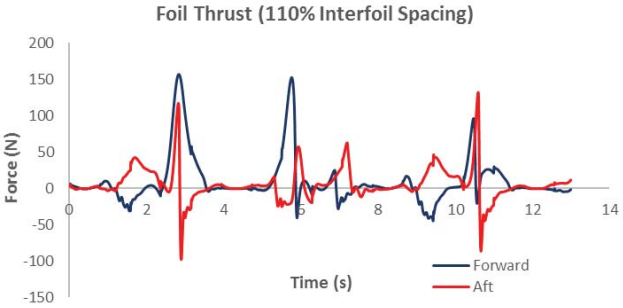

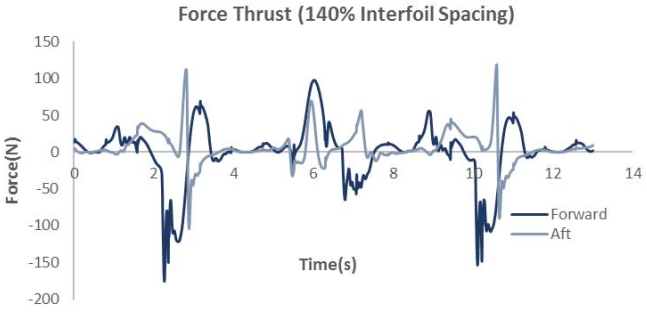

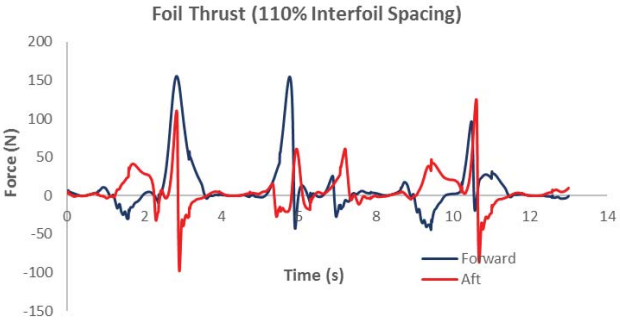

Graphs 32 to 35: Raw data obtained for foil thrust force at each interfoil spacing for prescribed pitch motion based on experimental data

Graphs 36 to 39: Raw data obtained for foil thrust force at each interfoil spacing for prescribed equal pitch motion +/-14 deg.

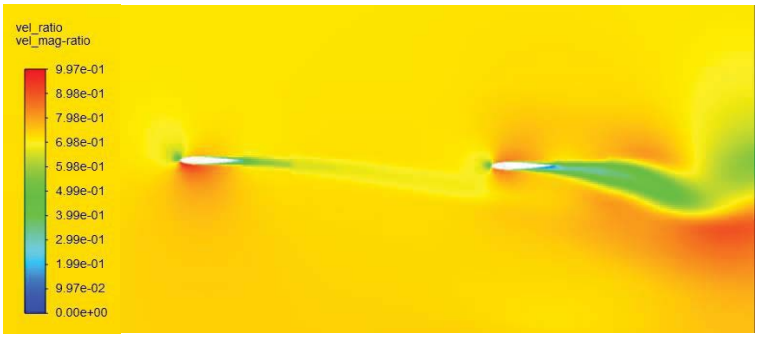

Time step: 40
Time: 0.4s
Inlet velocity: 0.334 m/s

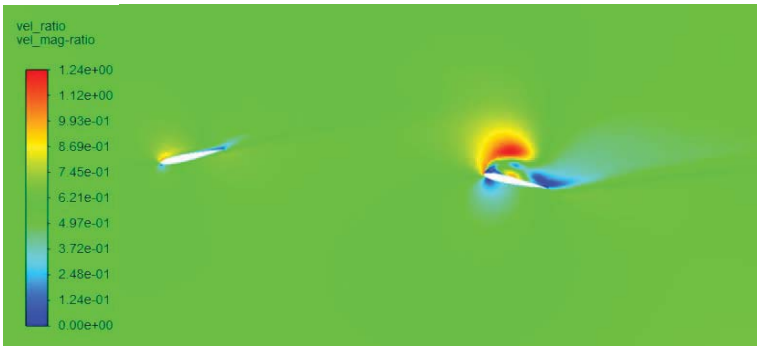

Time step: 80
Time: 0.8s
Inlet velocity: 0.298 m/s

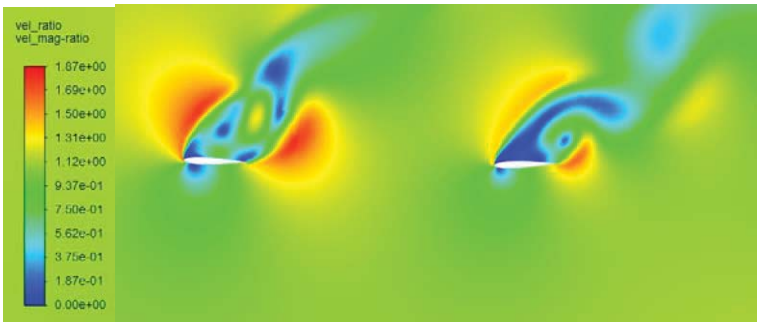

Time step: 120
Time: 1.2s
Inlet velocity: 0.521 m/s

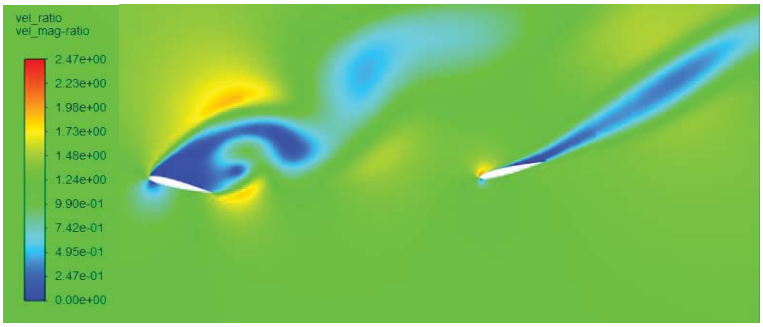

Time step: 160
Time: 1.6s
Inlet velocity: 0.582 m/s

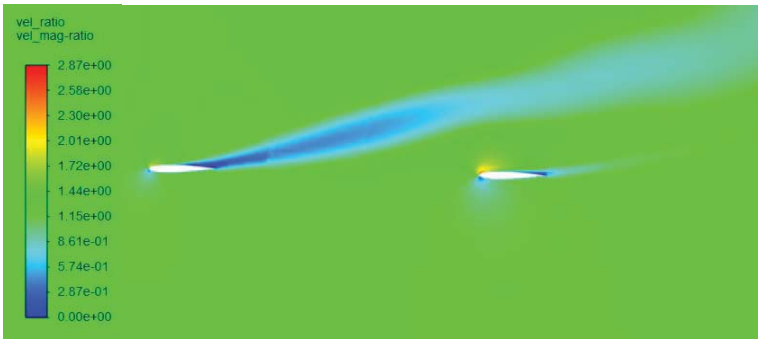

Time step: 200
Time: 2.0s
Inlet velocity: 0.589 m/s

Fig. 16 to 20: Contour plots velocity magnitude ratio $^{vel_{mag}}/_{vel_{inlet}}$*; A pitching cycle at 50% Interfoil Spacing, +/-14 deg. prescribed pitch motion*

Time step: 40
Time: 0.4s
Inlet velocity: 0.334m/s

Time step: 80
Time: 0.8s
Inlet velocity: 0.298m/s

Time step: 120
Time: 1.2s
Inlet velocity: 0.521m/s

Time step: 160
Time: 1.6s
Inlet velocity: 0.582m/s

Time step: 200
Time: 2.0s
Inlet velocity: 0.589m/s

Fig. 21 to 25: Contour plots velocity magnitude ratio $^{vel_{mag}}/_{vel_{inlet}}$*; A pitching cycle at 140% Interfoil Spacing, +/-14 deg. prescribed pitch motion*

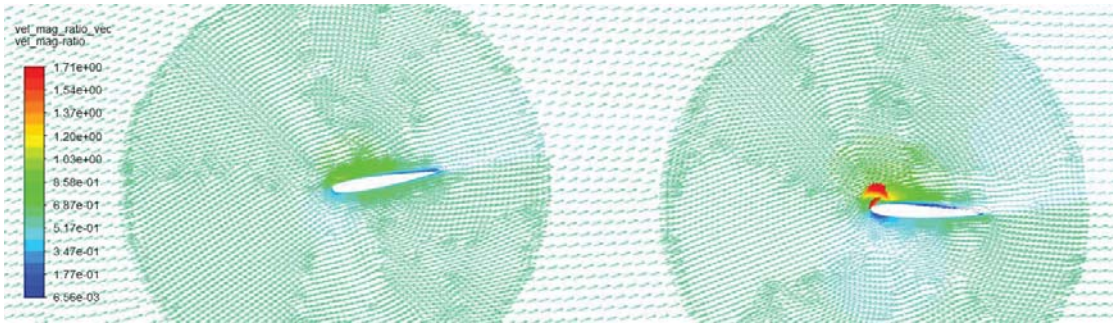

Time step: 77
Time: 0.77s
Inlet velocity: 0.297 m/s

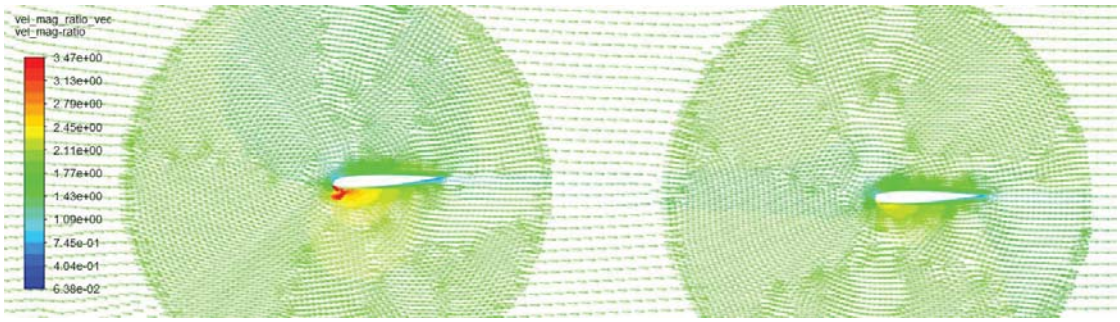

Time step: 254
Time: 2.54s
Inlet velocity: 0.816 m/s

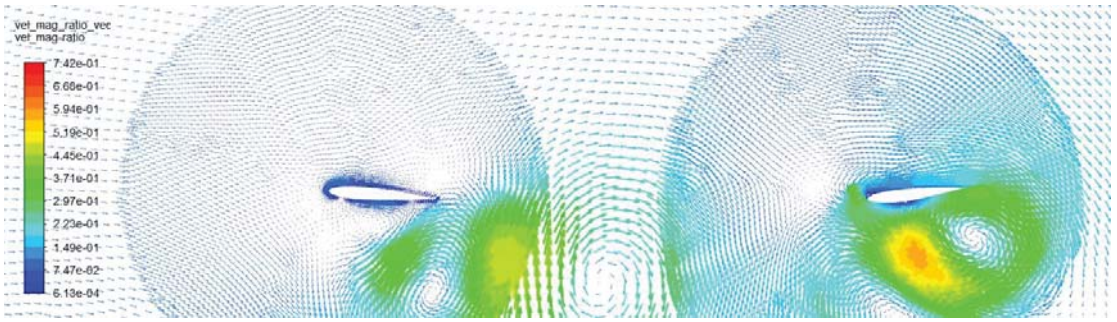

Time step: 432
Time: 4.32s
Inlet velocity: 0.051 m/s

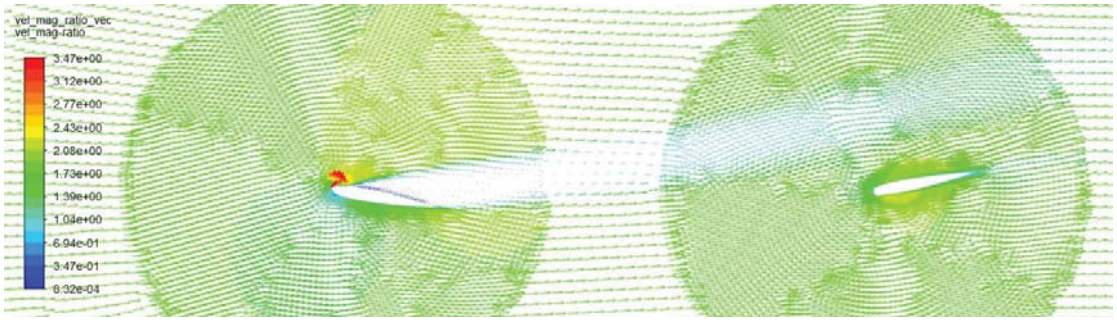

Time step: 609
Time: 6.09s
Inlet velocity: 0.822 m/s

Time step: 786
Time: 7.86s
Inlet velocity: 0.280 m/s

Fig. 26 to 30: Vector plots velocity magnitude ratio $^{vel_{mag}}/_{vel_{inlet}}$*; A wave cycle at 50% Interfoil Spacing, pitch motion prescribed based on experimental data*

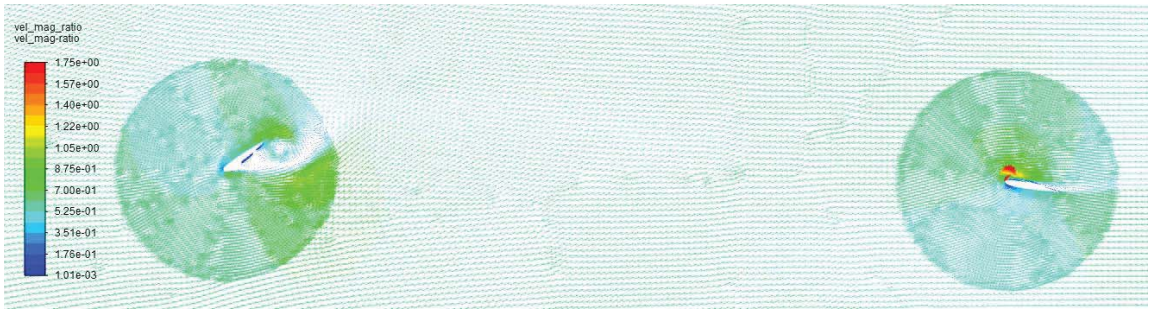

Time step: 77
Time: 0.77s
Inlet velocity: 0.297 m/s

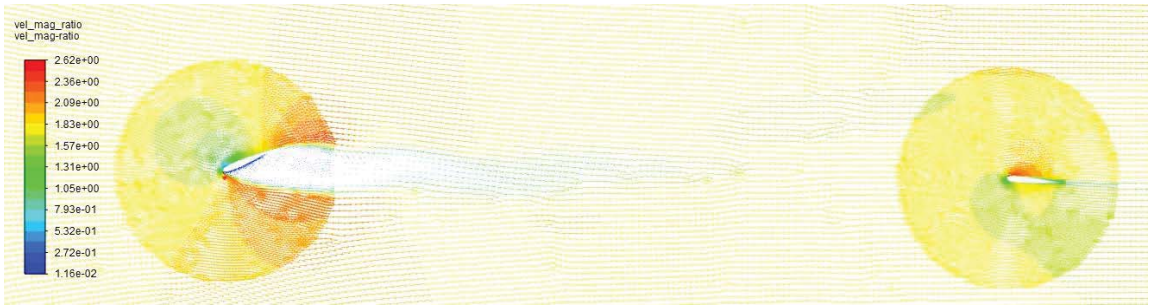

Time step: 254
Time: 2.54s
Inlet velocity: 0.816 m/s

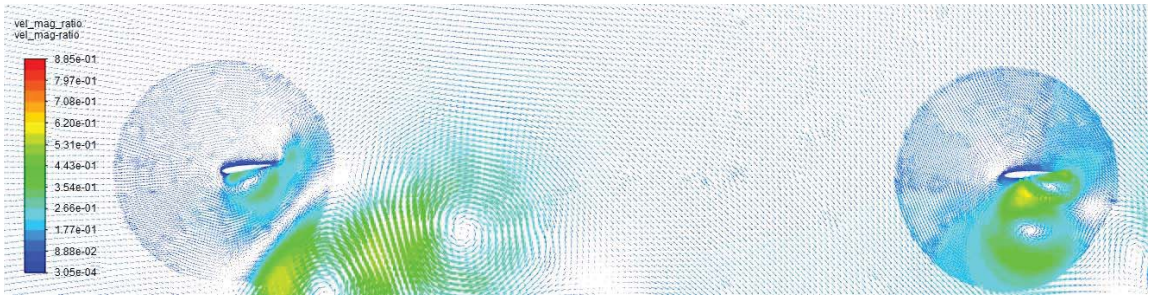

Time step: 432
Time: 4.32s
Inlet velocity: 0.051 m/s

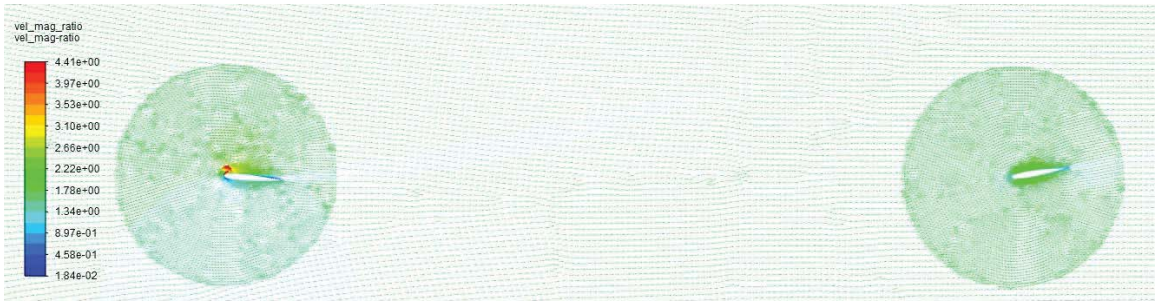

Time step: 609
Time: 6.09s
Inlet velocity: 0.822 m/s

Time step: 786
Time: 7.86s
Inlet velocity: 0.280 m/s

Fig. 31 to 35: Vector plots velocity magnitude ratio $^{vel_{mag}}/_{vel_{inlet}}$*; A wave cycle at 140% Interfoil Spacing, pitch motion prescribed based on experimental data*

Time step: 430
Time: 4.3s
Interfoil spacing: 50%

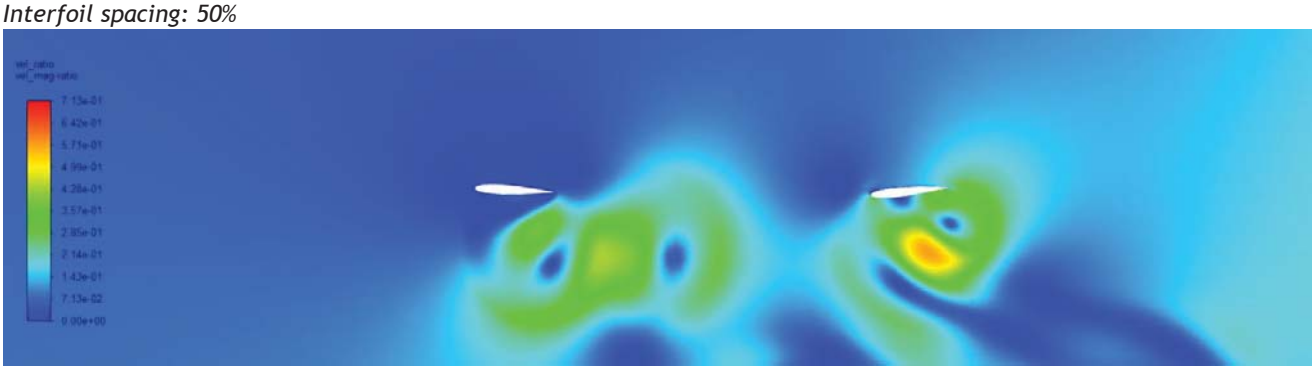

Interfoil spacing: 80%

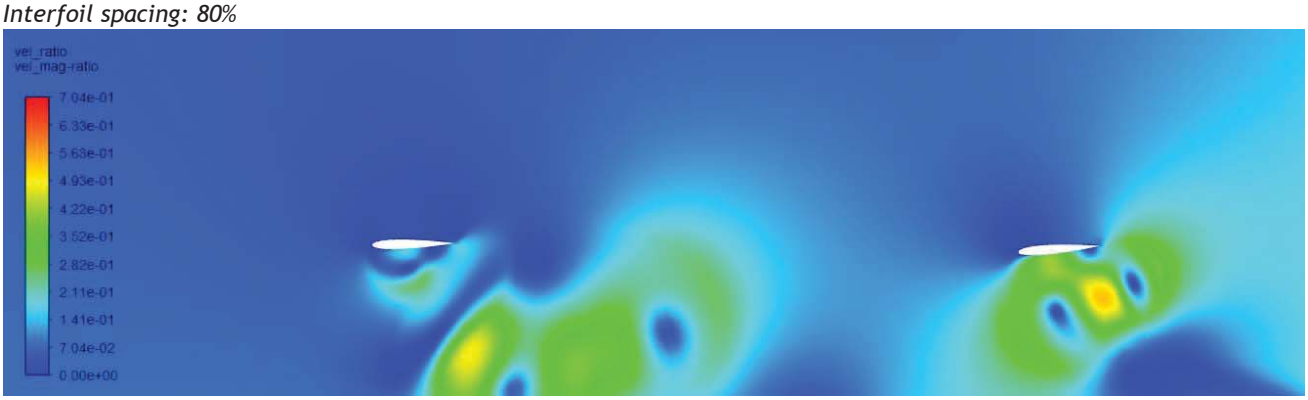

Interfoil spacing: 110%

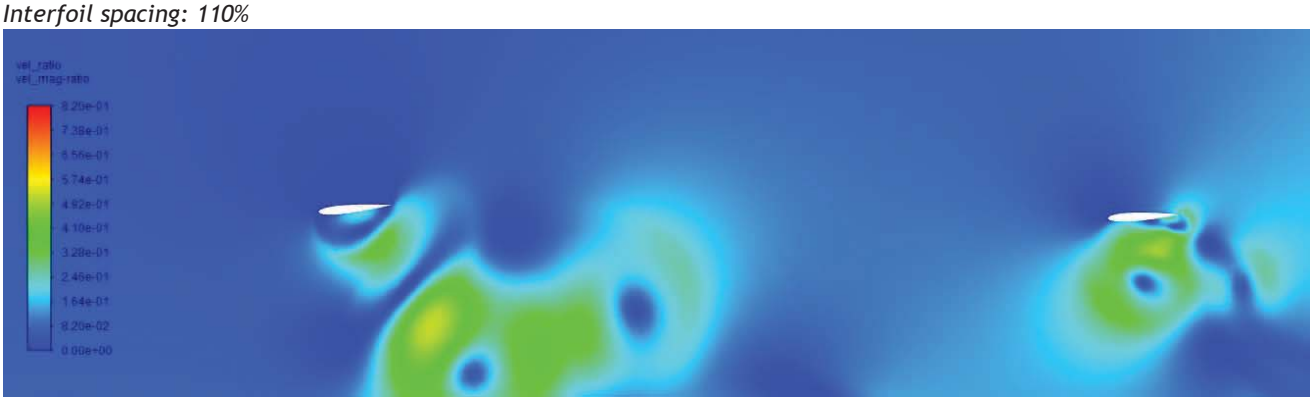

Interfoil spacing: 1140%

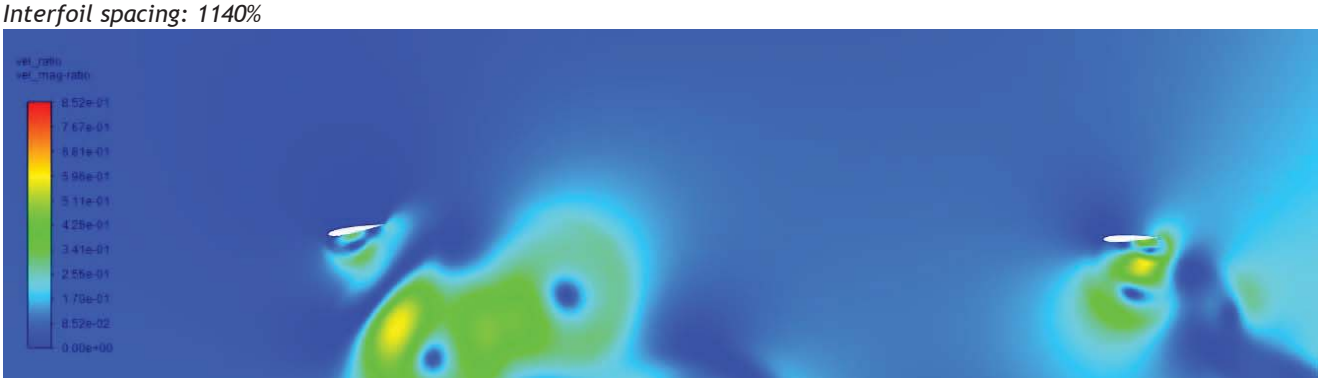

Fig. 36 to 39: Contour plots velocity magnitude ratio $^{vel_{mag}}/_{vel_{inlet}}$*; At minimum inlet velocity, prescribed pitch motion based on experimental data*

Time step: 594
Time: 5.94s
Interfoil spacing: 50%

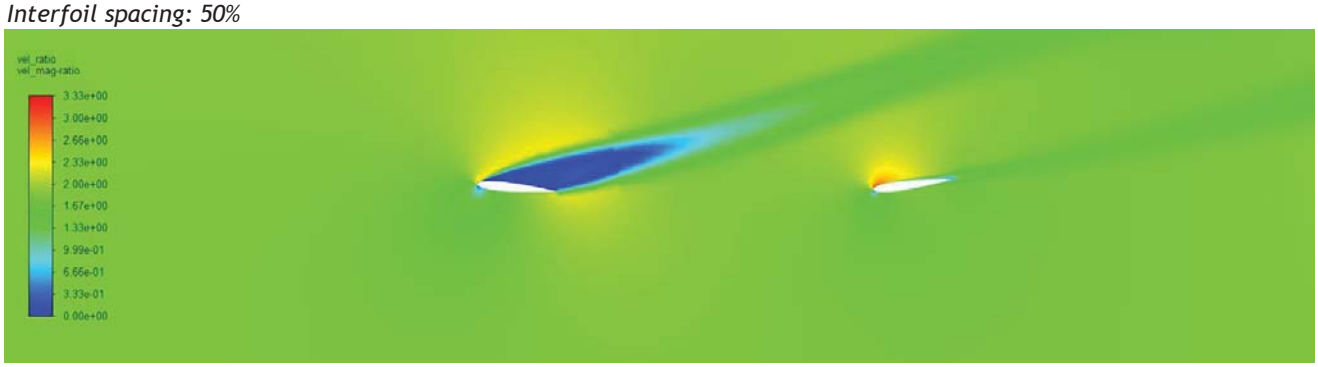

Interfoil spacing: 80%

Interfoil spacing: 110%

Interfoil spacing: 140%

Fig. 40 to 43: Contour plots velocity magnitude ratio $^{vel_{mag}}/_{vel_{inlet}}$*; At maximum inlet velocity, prescribed pitch motion based on experimental data*

Time step: 430
Time: 4.3s
Interfoil spacing: 50%

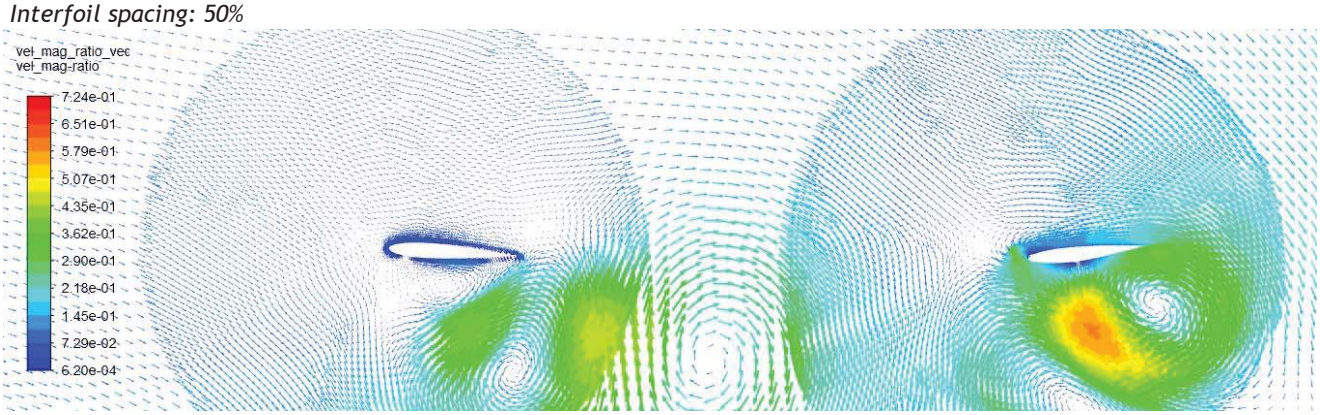

Interfoil spacing: 80%

Interfoil spacing: 110%

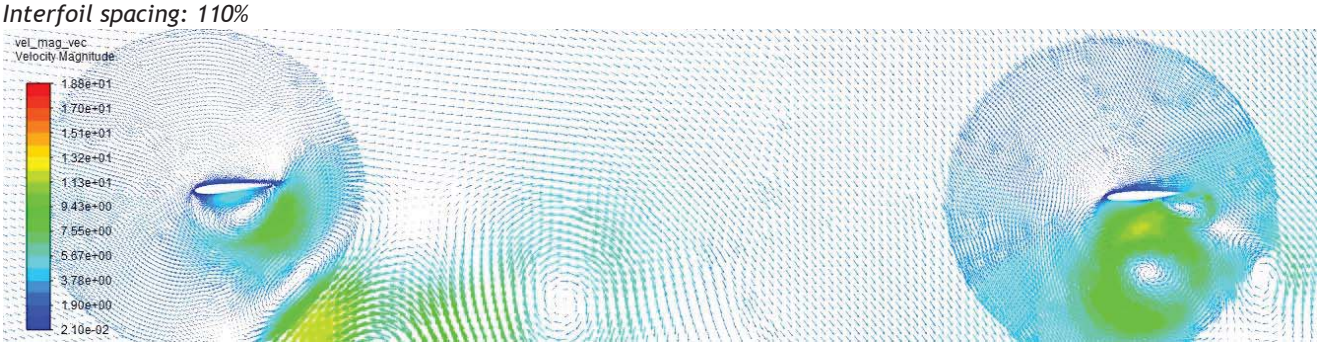

Interfoil spacing: 140%

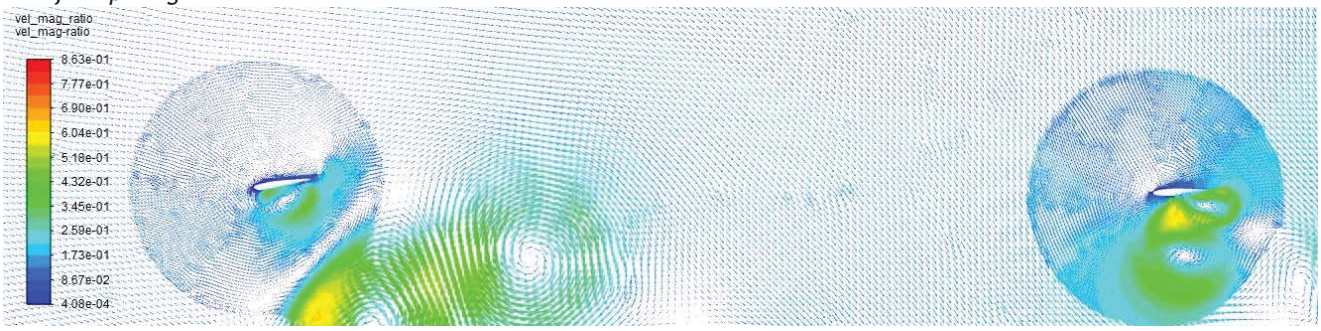

Fig. 44 to 47: Vector plots velocity magnitude ratio $^{vel_{mag}}/_{vel_{inlet}}$*; At minimum inlet velocity, prescribed pitch motion based on experimental data*

Time step: 594
Time: 5.94s
Interfoil spacing: 50%

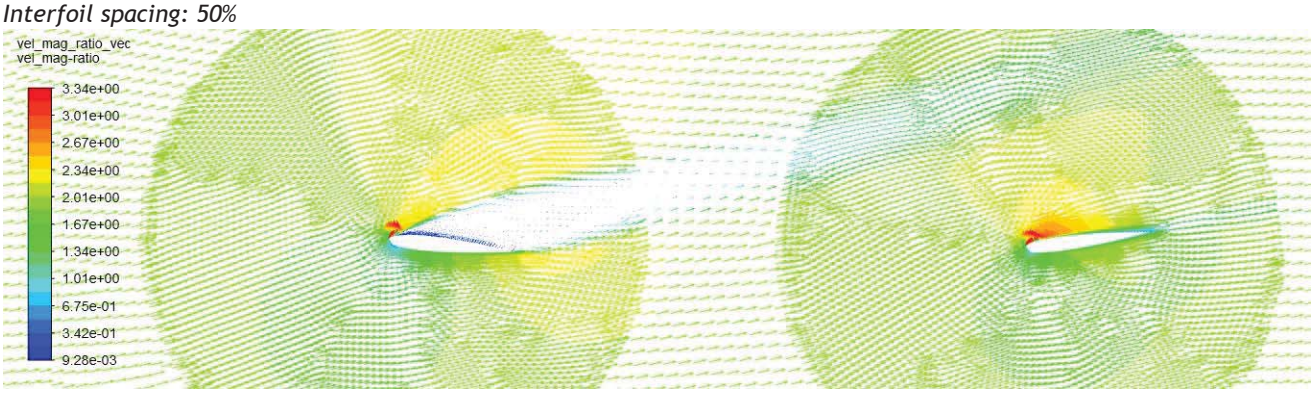

Interfoil spacing: 80%

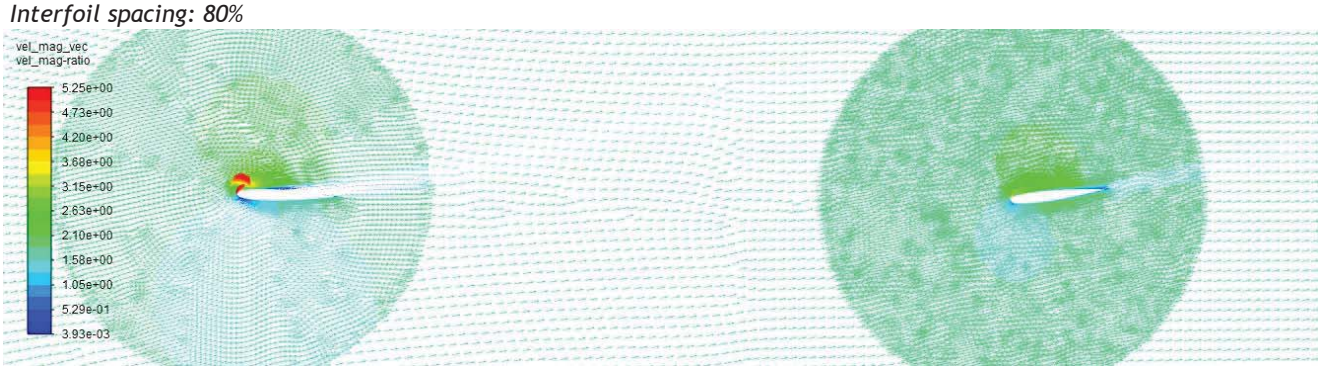

Interfoil spacing: 110%

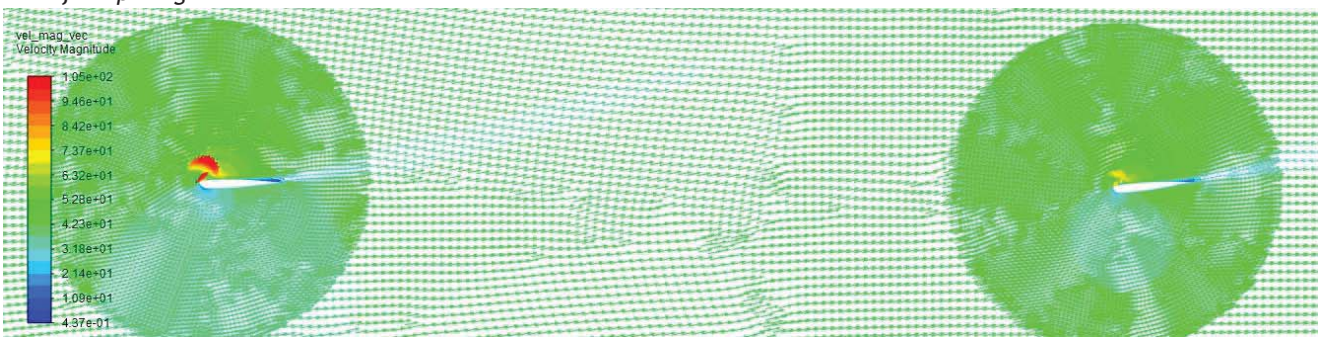

Interfoil spacing: 140%

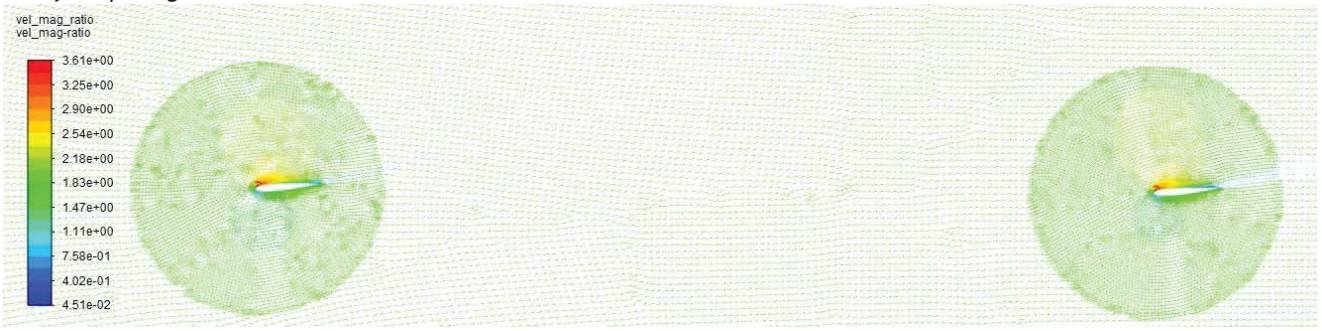

Fig. 48 to 51: Vector plots velocity magnitude ratio $^{vel_{mag}}/_{vel_{inlet}}$*; At maximum inlet velocity, prescribed pitch motion based on experimental data*